ACS Photonics

pubs.acs.org/journal/apchd5

Perspective

Space and Time Modulations of Light with Metasurfaces: Recent Progress and Future Prospects

Elena Mikheeva,‡ Christina Kyrou,‡ Fouad Bentata,‡ Samira Khadir, Sébastien Cueff, and Patrice Genevet*

Cite This: https://doi.org/10.1021/acsphotonics.1c01833

Read Online

ACCESS | Metrics & More | Article Recommendations

ABSTRACT: In this Perspective, we discuss the different opportunities offered by time-modulated metasurfaces for dynamic wavefront engineering and space-time photonics. Efforts in codesigning a photonic response while taking into careful consideration the switching/tuning mechanisms, including thermal, electronic, optical, chemical, and mechanical actuation, are essential for achieving sufficient amplitude, phase, and polarization modulation. Here, we examine in detail how the key enabling photonic technologies currently available and relying on similar tuning mechanisms can be applied for the conception of tunable metasurfaces. We review the latest developments and discuss the advantages and limitations of each approach, providing the reader with a clear vision of the current state of the art in active metasurfaces. We also address the readiness of each technological approach to drawing short- and long-term application perspectives. Finally, we discuss perspectives for spatiotemporal metasurface modulation opening new horizons toward unlimited wavefront engineering capabilities.

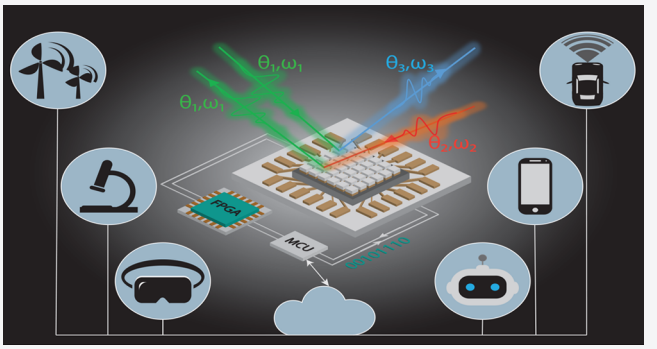

KEYWORDS: *tunable metasurfaces, reconfigurable metasurfaces, space−time modulation*

INTRODUCTION

Optical metasurfaces are ultrathin components made of a subwavelength arrangement of optical resonators or nanopillars designed with spatially varying structural properties (for more details, see review papers in refs 1−3). The variation of the geometry or material properties of these nanoscale elements often called optical building blocks, introduce a spatial variation on the reflected and transmitted electromagnetic fields. As a consequence, the reflected and/or transmitted light properties are modified. Various impressive results have been published over the last years, demonstrating phase, amplitude, and polarization encoding.[4−16] So far, we can classify the existing optical mechanisms of interest to achieve light modulation as follows: (1) the utilization of resonant scattering,[17] (2) the phase accumulation during light propagation in truncated waveguides,[18] where the transmitted phase ($\phi = 2\pi n_{\mathrm{eff}} h/\lambda$, n_{eff} and h represent, respectively, the effective index of the fundamental mode and the nanostructure height) is imparted by the mode of the nanostructure only, (3) the orientation-dependent phase retardation also called the Pancharatnam−Berry (PB) phase,[19,20] and (4) the recently proposed topological phase obtained by encircling optical singularities.[21] Resonant scattering designs can also be separated into local and nonlocal metasurfaces, depending on the nature of resonances excited in the structure (not to mix up with local and global external stimuli application). While local metasurfaces leverage the response of a single meta-unit (such as multipolar resonances or localized surface plasmons), nonlocal metasurfaces support collective modes in a periodic structure, such as guided-mode resonance in a substrate, surface lattice resonance, or quasi-bound states in the continuum. Nonlocal metasurfaces allow for the spectral tuning of a narrow band surface response, which might thus be advantageous for various applications.[22−25]

In a general case, metasurface building blocks are inherently passive, fabricated once and for all to perform a fixed optical functionality. While passive metasurfaces have extremely interesting application perspectives, in particular by considering their integration in optical and optoelectronic systems,[26−29] the optical responses of the components are not flexible. Efforts in achieving light modulation with ultrathin meta-

Received: November 30, 2021
Revised: March 10, 2022
Accepted: March 11, 2022

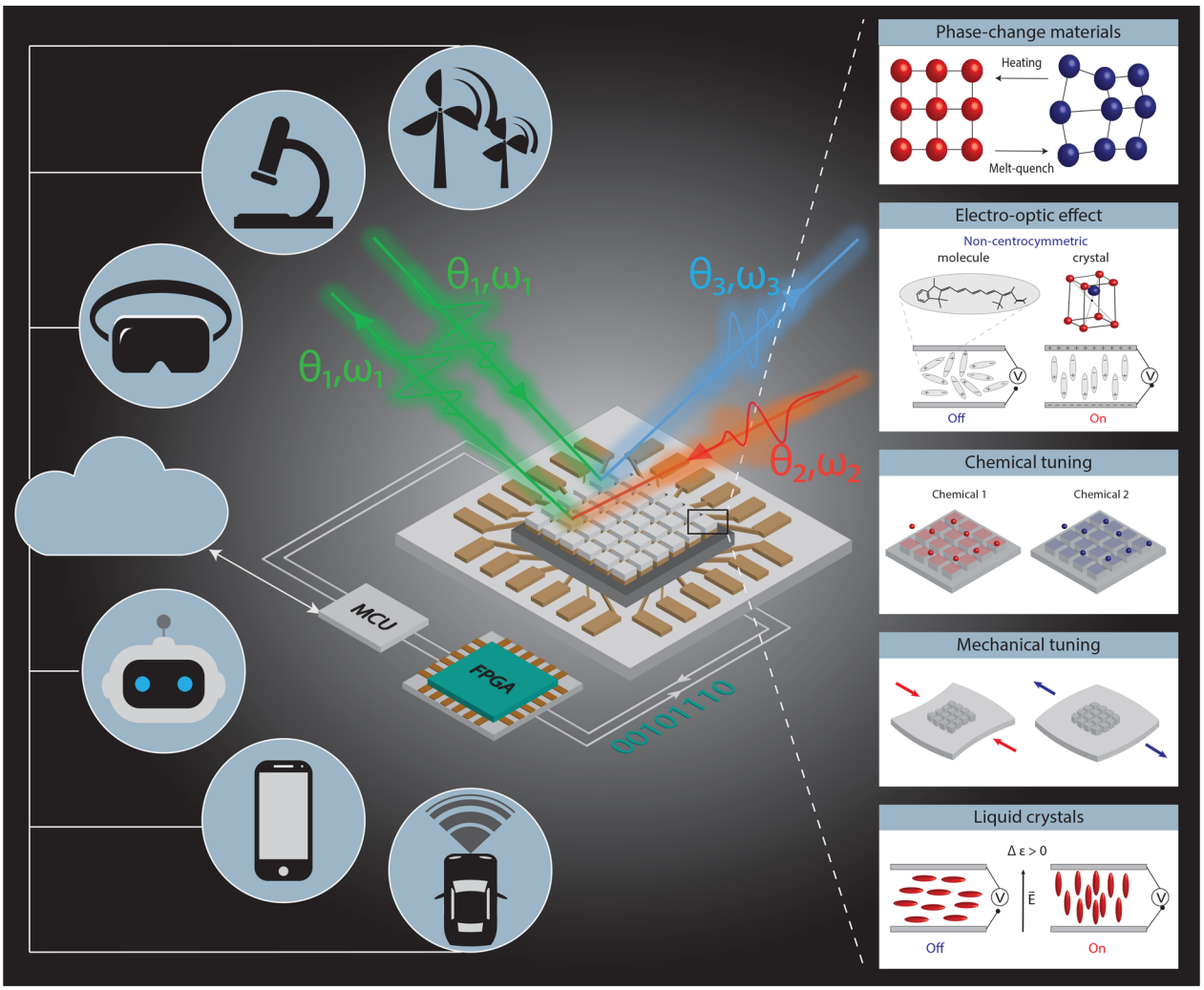

Figure 1. Schematic figure representing a dynamic metasurface that addresses space and time modulations. Several modulation mechanisms including phase-change materials, electro-optic effect, chemical tuning, mechanical tuning, and liquid crystals are illustrated on the right panel. Digital controllers and operation software dedicated to the complex metasurface architecture have to be considered in the future according to the applications of interest (left panel). Illustration of the optical effects obtained by breaking the reciprocity including nonreciprocal refraction and frequency modulation at interfaces (appears at high time modulation speed only).

surfaces would open serious research opportunities and unlimited industrial applications. The purpose of this Perspective is to summarize which are the enabling technologies that can be reasonably considered for achieving reconfigurable metasurfaces. Reconfigurable (also called active) metasurfaces have been realized long ago at microwave frequencies using active elements, such as PIN-diodes or varactors, as discussed in various articles.[30−37] However, as the wavelength scales down, this option is no longer available and tunability has to be introduced by changing either the properties of materials composing the metasurface building blocks or the optical properties of the surrounding medium using external stimuli. Several manuscripts have been published to categorize tunable metasurfaces, for example, by grouping them according to the tuning mechanism: electrical, mechanical, optical, thermal,[38] and chemical tuning.[39] It is possible to differentiate them according to the types of materials, such as transparent conductive oxides, ferroelectric materials, 2D materials (graphene, MoS_2), phase-change materials, liquid crystals, and semiconductors.[40] Other reviews have distinguished electro-mechanical switching[41] and free-carrier density modulation[42] into separate categories. In addition to thoroughly discussing different tuning mechanisms, one of the previous reviews also provides an insight into applications of dynamic metasurfaces, in particular, focusing on spatiotemporal devices.[43] Another reported review divides tunable metasurfaces into hybridized ones (e.g., combining active medium with metals) and metasurfaces with building blocks made of active material.[44] Here, we propose to draw prospects of this research field by analyzing how the existing technologies help improve the level of development of tunable metasurfaces and how they help bridge the gap between academic research and industrial applications.

Figure 1 summarizes schematically the content of this Perspective. It shows a programmable metasurface featuring an arbitrary electromagnetic response in space and time activated using different tuning mechanisms. On the right panel of Figure 1 we show a selection of perspective tuning mechanisms, including phase change materials, electro-optic effect, chemical reactions, mechanical tuning, and liquid crystal reorientation. Their advantages and bottlenecks and their potential for large-scale industrialization are discussed in the

https://doi.org/10.1021/acsphotonics.1c01833
ACS Photonics XXXX, XXX, XXX−XXX

Table 1. Key Metrics for Different PCMs: Complex Refractive Index at Two Wavelengths, 630 and 1550 nm (from Left to Right: Minimum Real Part of Refractive Index, Contrast Δn between the Crystalline and Amorphous States, Extinction Coefficient at the Crystalline State), Switching Temperature, Energy Density (the Switching Energy per Unit PCM Volume), and Switching Speed[a]

	n_{min}, Δn, k_c				
PCM	λ = 630 nm	λ = 1550 nm	T_c (°C)	switch energy	switch speed
GST	3.63, 0.52, 3.72	3.63, 2.1, 1.8	180	1.3×10^{-2} fJ/nm^3	50 ns
VO_2	2.56, 0.1, 0.3	1.36, 1.4, 2.9	70	1.5×10^{-9} fJ/nm^3	~ns−μs
GSST	3.7, 1.9, 2	3.21, 1.8, 0.3	400	2.2×10^{-2} fJ/nm^3	100 ms
Sb_2S_3	3.11, 0.89, 0.58	2.69, 0.54, 0	280	5.9×10^{-2} fJ/nm^3	75 ns
Sb_2Se_3	4.4, 1.17, 1.27	3.7, 0.7, 0	200	7.9×10^{-2} fJ/nm^3	100 ms

[a]The energy densities and switching speeds were found to strongly depend on the design and switching mechanism (optical or electrical), as well as on the preparation methods and deposition conditions, refs 53−56. The values reported here should therefore not be seen as fundamental ones, but rather as state-of-the-art metrics that we collected from different works[56−62] that we find representative of the different values reported in the literature.

first part of this Perspective. The success in the implementation and integration of these devices in complex systems relies on their compatibility with well-established, low-cost, and scalable manufacturing processes. Voltage addressing using electronic elements and driving integrated circuits (ICs) has been selected as probably one of the most, if not the most, promising routes for active metasurfaces. Figure 1 illustrates schematically a time-varying metasurface based on different tuning mechanisms and its possible applications. Time-varying functionality is achieved by applying external stimuli such as electrical bias. Electronic devices providing real-time digital modulated voltage outputs, such as a field-programmable gate array (FPGA), can switch the states of the meta-units. Real-time programming of the metasurface requires, for instance, a microcontroller unit (MCU) equipped with an advanced driving algorithm to regulate the FPGA outputs. This device aligns very well with the current quest in the industry for achieving a high degree of automation in decision-making. Internet-of-Things (IoT) and Autonomy-of-Things (AoT) are driving the high demand in systems offering high-end synchronization and intercommunication, and we believe that active metasurfaces could certainly offer interesting application perspectives in these areas. These applications include LiDAR (Light imaging Detection and Ranging) sensors for advanced assisted driving systems (ADAS) or even fully autonomous driving,[45] wearable devices for AR/VR applications,[25] robotic industry 4.0,[46] microscopy and image treatment,[22] and so on. We finally provide insights on academic and relatively unexplored research topics dealing with spatiotemporal metasurfaces. We illustrate a nonreciprocal metasurface that can be realized in the case of ultrafast time modulation, that is, a device in which time-reversal symmetry is broken and that enables asymmetric trajectories accompanied by frequency shifting. We show an example of nonreciprocity together with others to illustrate the versatility and diversity of applications of tunable metasurfaces.

FROM CURRENT KEY ENABLING TECHNOLOGIES TO TUNABLE METASURFACES

From Phase-Change Memories to Active Metasurfaces. Phase-change materials (PCMs) for photonics have been a booming field of research for roughly a decade.[47] The tantalizing potential of PCMs for dynamic metasurfaces can immediately be understood by summarizing their most salient features: (i) large refractive index modulation (one of the largest compared to other considered tuning mechanisms, $\Delta n \geq 1$, as shown in Table 1), (ii) fast, reversible, and for some of them nonvolatile switching, (iii) multistimuli switching (thermal, optical, electrical, and so on), and (iv) potential monolithic integration at the nanoscale.

The large body of research on PCMs for photonics is described in a few reviews that can be found in the literature (see, e.g., refs 47−50), some of which are entirely dedicated to PCM for metasurfaces.[51,52] Most of these reviews are focused on "standard" PCMs, such as chalcogenide PCMs (GeSbTe or GeTe), or phase-transition oxides, such as VO_2. Very recently, a new category of PCMs, which we hereby call "low-loss PCMs", has emerged, comprising three main materials: Sb_2S_3, Sb_2Se_3, and GeSbSeTe. Given the advantageous properties of these emerging materials, they have the potential to outclass standard PCMs. After reviewing very recent results obtained on standard PCMs, we, therefore, dedicate a large part of this subsection to recent works exploiting the low-loss PCMs for metasurfaces.

Standard PCMs. PCMs are unique materials whose physical properties depend on their crystallographic states. Two classes of materials are usually referred to as PCMs: chalcogenide PCMs (e.g., GeSbTe) and phase-transition oxides (e.g., VO_2). These two categories share similarities in that a modification of their structural atomic arrangements produces large modulations of their complex refractive indices (Table 1). However, the underlying physics behind their respective modulations is different (for this reason, some researchers consider that they should not be grouped under the same label of PCM). We briefly describe below the basic physical principles that produce such drastic physical modulations.

VO_2 presents a first-order transition from a monoclinic insulating state at room temperature to a tetragonal metallic state at temperatures above 70 °C. This material is a famous example of Mott insulators: according to band theory, it should be a metal, but experimentally it behaves as an insulator. The physical reason behind this phenomenon is strong electron correlations between free carriers that prevent electrical conduction.[50,63] A moderate input of energy into that system can break the equilibrium and trigger a transition from an insulating state to a conductive state. This so-called insulator-to-metal transition happens in a very short time (down to the femtosecond time scale).[64−66] Conversely, the metallic state is volatile and, hence, switching back from metallic to insulating is typically slower, as it requires evacuating the excess energy/heat brought by the first excitation. Note that the on−off

https://doi.org/10.1021/acsphotonics.1c01833
ACS Photonics XXXX, XXX, XXX−XXX

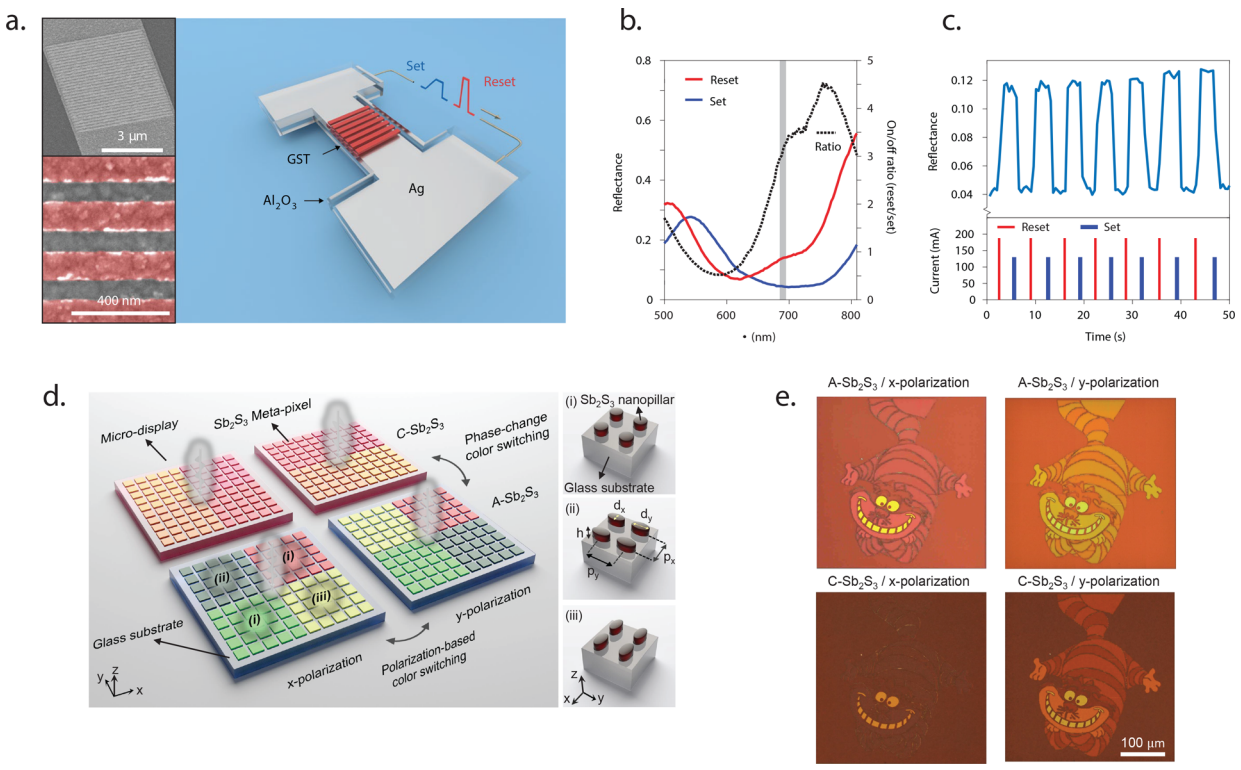

Figure 2. Highlights: Metasurfaces based on phase-change materials. (a) Tunable GST metasurface placed on optically thick silver stage which is heated by set and reset current pulses. This leads to GST meta-atoms being switched between amorphous and crystalline states. (b) Experimental reflection spectra for the metasurface from (a) being set and reset with current pulses. (c) Demonstration of switching metasurface from (a) in time between reflecting and absorbing states corresponding to set and reset conditions from (b). (a–c) Republished with permission of Springer Nature from ref 90. Copyright 2021 Springer Nature; permission conveyed through CCC, Inc. (d) Reflective color displays consisting of low-loss PCM Sb_2S_3 anisotropic particles arranged periodically and forming meta-pixels. Each meta-pixel produces different colors for 2 perpendicular linear polarization, both produced colors can be tuned by switching Sb_2S_3 pillars with an on-chip heater made of conductive transparent oxide. (e) Images obtained by using the structure shown in (d) with meta-pixels in the amorphous and crystalline state for *x*- and *y*-polarization. (d, e) Reprinted with permission from ref 96. Copyright 2021 Ali Adibi.

switching cycle is accompanied by a hysteretic behavior that can prove useful for some applications.

VO_2 is widely used for its tunable plasmonic resonance in the metallic state that switches off in the insulating state in the IR.[67−69] Recent papers show that nanostructures made of or combined with VO_2 exhibit Mie resonances in both insulating and metallic states, opening the door for new metasurface designs such as tunable Huygens Metasurfaces in both the visible and near-infrared ranges.[70−72] As mentioned previously, the transition can also be controlled by electrical means. Based on that principle, spectral modulation[73] and optical phase modulation[74] were recently demonstrated using electrically driven VO_2-based metasurfaces operating around the telecom wavelength range. Apart from all the mentioned designs, thermally tunable VO_2-based absorbers were also successfully implemented.[75,76] Additionally, the metastable metallic state, even though volatile, can be used at an advantage to optically or electrically write devices with large flexibility and ease to erase. This phenomenon was used to demonstrate an optically rewritable photonic 'metacanvas' in which the hysteresis was used as a means to hold the metallic patterns by maintaining the sample at a moderate temperature (70 °C).[77] Using this method, arbitrary patterns for diverse optical responses can be written and erased very easily. Given the lower optical absorption of insulating VO_2 in the mid-infrared and THz ranges, several recent works reported efficient electrically controlled multifunctional amplitude switching VO_2-based metasurfaces in these wavelength ranges.[78,79]

The other class of PCMs, chalcogenide-based PCMs, possess properties typical of a semiconductor when it is amorphous: a moderate refractive index and a dielectric nature. However, when the same material is crystallized, its refractive index becomes very large and the material becomes conductive. Such behavior is very much unlike conventional materials (e.g., amorphous and crystalline silicon) and is due to an unconventional bonding mechanism in the crystalline state, recently coined "metavalent bonding".[80,81] Chalcogenide PCMs can be composed using alloys of germanium (Ge), antimony (Sb), tellurium (Te), selenide (Se), and sulfur (S). This creates a library from which materials can be selected based on the bandgap, complex refractive index, and required properties.[40] Among them, germanium−antimony−telluride ($Ge_xSb_yTe_z$ with various stoichiometry) is one of the most studied PCMs for photonics. It has high cyclability (10^{15}), high switching speed, high retention (~10 years), and low power consumption, depending on the unit cell size.[51,82,83]

Provided the switching of chalcogenide PCM physical properties is governed by their crystallization, such modulation is by definition nonvolatile. It is also reversible through a reamorphization process that is usually obtained by a melt-quenching method in which a PCM is heated above its fusion point and subsequently cooled down at rates faster than the crystallization kinetics (more than 10^9 Ks^{-1} for GST).[47,84]

https://doi.org/10.1021/acsphotonics.1c01833
ACS Photonics XXXX, XXX, XXX−XXX

Reamorphization is an extremely fast process that can be triggered by a single-pulse femtosecond laser or nanosecond electrical pulse. The overall cycling time is limited by the crystallization process, which is slower than the amorphization.

There are several ways to switch these materials between states, such as thermal annealing[84,85] or optical writing with pulsed lasers.[86,87] However, one of the most important mechanisms is electrical switching, as it promises future integration with other microelectronic technologies. This kind of switching is well-developed for phase-change random-access memory (PC-RAM) technology that has a data transfer rate greater than gigahertz (having ∼10 nm cells).[88,89] However, scaling it up to ∼100 nm and larger sizes becomes challenging due to a nonuniform phase transition within a bulk of PCM, especially for a cooling process. This problem has been addressed with electro-thermal switching of metasurfaces, which opened a route to codesigned photonic and electronic devices.[56,90−92]

In particular, electro-thermal switching leveraging an integrated microheater layer provide an efficient means to locally tune PCMs. Wang et al. recently demonstrated a GST-based metasurface placed on top of a thin silver film (Figure 2a) that plays both the role of a plasmonic antenna and a microheater that uniformly heats the structure (unlike direct current injection with a filament in PC-RAM).[90] Both crystallization and amorphization are carried out by running current pulses: a lower current pulse with a longer duration crystallizes the PCM, while shorter and higher current pulse leads to reamorphization. The metasurface acts as a perfect absorber when GST is crystalline (due to destructive fields interference) and starts reflecting light when it is amorphous. Experimental results show reflection switching from ≈4.3% to ≈14.5% at 700 nm wavelength, as shown in Figure 2b. The authors report a 10 kHz modulation speed for this hybrid PCM metasurface (Figure 2c). Abdollahramezani et al. also recently demonstrated electrical switching of the hybrid GST-Au metasurface supporting two distinct plasmonic modes that can be tuned by the GST layer, hence, modulating the reflection amplitude in the NIR. The device exploits a tungsten microheater enabling an electrical control of the crystallization state of the GST layer.[93]

An alternative recent strategy for phase transition is the solid−liquid phase transition. Bismuth nanostructures are nanoparticles based on the bismuth monoelement used because of its solid−liquid optical contrast with low melting points of about 270 °C. Recently, Alvarez-Algeria et al.[94] demonstrated the relevant properties of a random distribution of Bismuth-nanostructures in a dielectric matrix (PCRMs, phase change random metasurfaces). A nanosecond pulsed laser was used to melt the Bismuth-nanostructures with different filling factors, allowing a high optical contrast between the solid and liquid states (on/off state) and fast switching up to 10 ns and semivolatile behavior, which means staying at the melting phase without a permanent power supply for a given time duration. This was enabled by using latent heat to maintain the temperature at phase transition and by designing the distance between the Bismuth-nanostructures and the Si substrate, which also plays a heating role that lengthens the melting time and thus the melting phase >1 μs (on-state) and high cyclability up to 100000 cycles without damaging the sample.

Emerging Low-Loss PCMs. The standard PCMs, such as GST and VO_2, present a high optical absorption in the visible and NIR spectral range, which limits their utilization in realistic optical systems. Recently, alternative low-loss materials with high contrast in the refractive index and low extinction coefficient in the visible and NIR regime have emerged.[60−62,95,96] For example, Sb_2S_3 presents a transparency window from 610 nm to the NIR with a relatively large index contrast and cyclability higher than 1000 cycles,[60] and Sb_2Se_3 has a transparency window from 800 nm to the NIR, a larger index contrast and relatively high cyclability (4000 cycles).

High refractive index and transparency make Sb_2S_3 and Sb_2Se_3 good candidates for electronic displays or meta-screens.[96] Recent works report such meta-displays designed using anisotropic pillars supporting multipolar resonances, as shown in Figure 2d. A single metascreen can generate two colors for two different polarizations of visible light that can be switched when PCM changes between its amorphous and crystalline states. Figure 2e shows two different images for two perpendicular linear polarization for the amorphous phase. Switching these parameters changes the display colors and, with the right optimization, makes a part of the image disappear.

As in the case of GST discussed previously, designing the heating element for low-loss PCMs is an important step to providing a uniform heat flow to the meta-atoms, in order to increase the switching capabilities (e.g., reversibility) and to optimize the power supply without compromising the optical efficiency. For example, Zhang et al.[56] used a gold thin film that acts both as a heater and an optical reflector for their GSST-based metasurface. The design of the microheater includes a curved shape and a larger surface area than the metasurface, allowing a directional current flow and a uniform heat distribution to the meta-atoms. Interestingly, the slower crystallization kinetics of GSST compared to GST enables optimizing the heat distrtibution, reducing the power loss around the telecommunication wavelength (about 1.5 μm) and using a larger thickness of PCMs (about 250 nm).

These very promising recent results combine both low-loss PCMs with electrical control of their crystallization state. So far, the architecture of these first demonstrations can only enable the switching of devices as a whole. Said otherwise, they cannot provide direct control over each individual meta-atoms. Such an individual control of elements was recently demonstrated by optical means using an external laser to switch separate PCM-based meta-atoms.[97] While there are no fundamental limitations to direct electrical control of individual PCM meta-atoms, the current technical bottleneck is common for all the tuning mechanisms: how to electrically connect and independently drive thousands of nanoelements? One plausible route is to revisit current phase-change random access memories (PC-RAM). Such PCMs as GST are compatible today with 300 mm industrialization and ST microelectronics already demonstrated phase-change-based RAM integrating millions of nanoheater-controlled PCM cells, each addressed via an independent transistor in 28 nm FDSOI eNVM technology for automotive microcontroller applications.[89,98] The typical dimension of a nanoheater cell is around 50 nm, separated by around 100 nm, that is subwavelength dimensions in the visible. This ensures that pixel-by-pixel tuning using nanoheater is a promising approach for the realization of tunable metasurfaces at optical wavelengths.

Compacting Electrical Modulators to Functional Surfaces. *Metasurfaces Based on the Electro-Optic Effect.*

https://doi.org/10.1021/acsphotonics.1c01833
ACS Photonics XXXX, XXX, XXX−XXX

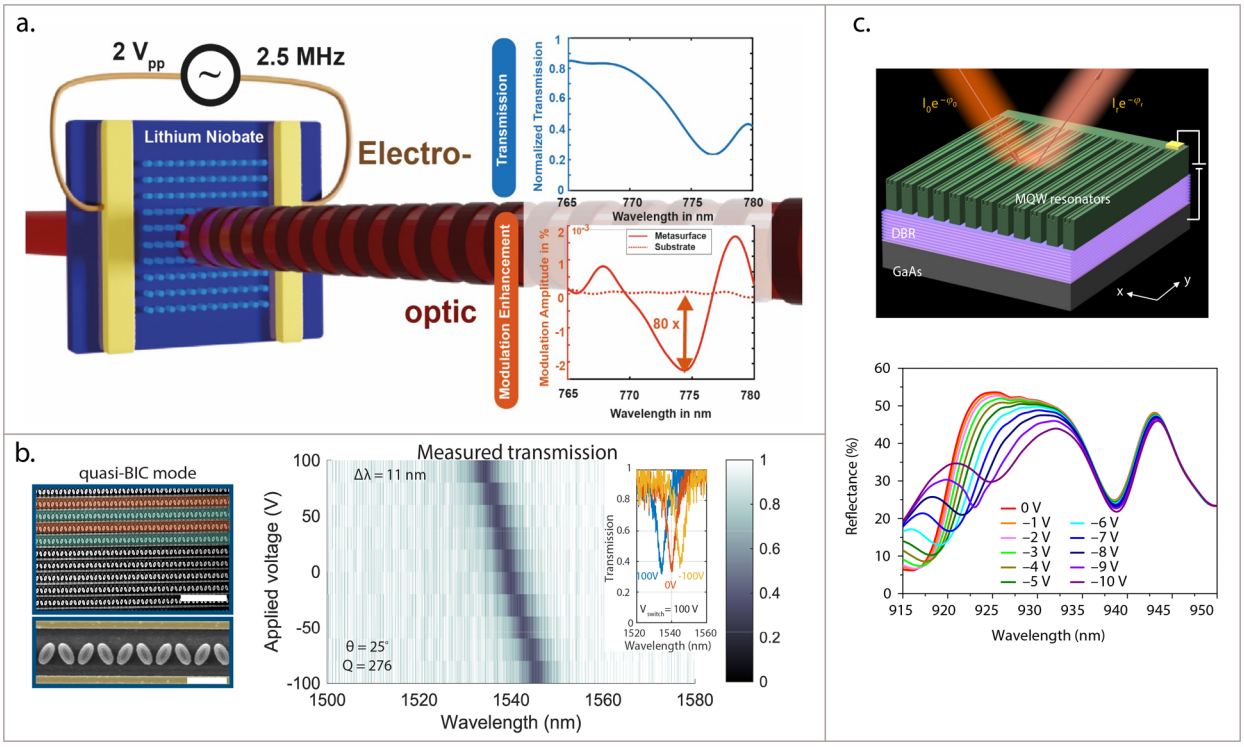

Figure 3. Electro-optic effect in lithium niobate resonators is used to achieve tunable metasurfaces with an extremely interesting transmission modulation speed up to 2.5 MHz. Reprinted with permission from ref 103. Copyright 2021 ACS Publications. (b) Metasurfaces consisting of quasi-BIC resonant nanoparticles produce high quality factor resonances embedded into a polymer supporting a linear electro-optic effect, also known as the Pockels effect. Results demonstrate the transmission amplitude modulation with a speed of up to 5 GHz. Reprinted with permission from ref 105. Copyright 2021 Federico Capasso. (c) Metasurface consisting of an n-doped GaAs substrate, a Bragg reflector, and a multiple-quantum-well resonator operating using a quantum-confined Stark effect modulation. The bottom figure shows reflectance spectra measured at different bias voltages. It is shown that, around λ = 917 nm, for a wavelength close to the interband transition of the quantum well, the reflection modulation is considerable. Reprinted with permission from ref 107. Copyright 2019 Springer Nature. Distributed under a CC BY 4.0 license https://creativecommons.org/licenses/by/4.0/.

Up to date, one of the best performances in terms of switching speed and low material loss for conventional optoelectronic devices have been achieved with electro-optical modulators, making use of the electro-optic (EO) effect. Considering the EO effect at the nanoscale for tunable optical metasurfaces would allow decreasing distance between the electrodes and lower the electrical power required to address the modulation. The EO effect includes the Franz−Keldysh effect (shift of the semiconductor absorption edge), the Stark effect (splitting and shifting of energy levels in a quantum system, could be linear and nonlinear), and Pockels and Kerr effects (linear and nonlinear birefringence induced by an electric field).[99]

In particular, the Pockels effect is currently used in many light-modulation applications. It is generally present in noncentrosymmetric materials (crystals, polymers, metal-oxide materials) and the degree of induced changes depends on the electro-optic tensor defined by the material's structural properties. In such a material, the electric field introduces linear refractive index shift along one of the crystallographic axes, while maintaining the same refractive index along orthogonal axes. The refractive index change depends on the applied voltage amplitude and polarity, getting oriented due to the superposition of different forces. The shift introduces phase retardation between different polarization components and achieves dynamic control of the light properties. As the induced refractive index change is generally very small, large phase or amplitude modulation using conventional optoelectronic devices requires propagating and thus modulating the transmitting phase through a sufficient thickness.

The resonant feature of metasurfaces might open the route to reduce the size of electro-optic crystals while providing sufficient phase and amplitude modulation. EO materials were used in combination with metals, serving as an embedding medium surrounding resonant plasmonic structure[100] as a part of metal−insulator−metal structure,[101] or as a nanoparticle layer combined with plasmonic nanostructures.[102] This metasurface already modulates reflection amplitude in the range of about 15% for a relatively low actuation voltage of about 4 V and at an extremely high modulation cutoff frequency of about 20 MHz.

Several current attempts to apply Pockels effects focused on using EO materials as resonant units, including the recently demonstrated metasurface made of lithium niobate crystal cylindrical posts.[103] Nanostructuring the lithium niobate thin film leads to lower-order multipolar resonances (in particular, resonance dominated by the electric dipole mode). By placing this structured surface between the electrodes (Figure 3a) and applying the AC driving signal, the resonance position is shifted, leading to a significant transmission modulation. In particular, by applying a 180 kHz signal with a peak-to-peak voltage 2 V_{pp}, it is possible to achieve an 80× larger modulation around the resonance compared with the unstructured film. Although the currently reported modulation depth remains small with respect to other mechanisms (0.002% at 2 V_{pp} and up to 0.01% at 10 V_{pp}), it enables a

https://doi.org/10.1021/acsphotonics.1c01833
ACS Photonics XXXX, XXX, XXX−XXX

large working bandwidth from 10 Hz to 2.5 MHz for a relatively small actuation voltage of 1 V_{pp}. The modulation performance could be further improved by optimizing the overlap between both electric fields induced by a modulating signal and the optical illumination.

Another way to improve performance, that is, enhancing the induced transmission modulation and reducing the voltage required for the EO-switching, is to use nonlocal metasurfaces supporting high-quality factor resonances. For example, quasi-bound states in the continuum (q-BIC) in lithium niobate metagratings predict high phase modulation compared to the unstructured film.[104] However, material losses and structural imperfections significantly lower the experimental q-BIC quality factor and lead to an only 1.46× larger modulation with respect to the homogeneous film. Another example of active spectral tuning of q-BIC states is realized using silicon resonators covered by a polymer with dispersed EO-molecules (active JRD1/PMMA layer).[105] It employs second-order nonlinear materials exhibiting a linear EO effect as a surrounding for meta-atoms supporting high-quality factor resonances designed by symmetry breaking. Each unit cell consists of two ellipses that are rotated with respect to the vertical axis, as shown in Figure 3b (right). The angle of rotation allows controlling the resonance quality factor. By applying voltage, polar molecules are aligned, which changes the refractive index components, resulting in the q-BIC resonance shift, as shown in Figure 3b (left). This metasurface modulates light with one of the highest switching speeds reported to date (up to 5 GHz). The authors, among other results, also reported a voltage reduction from 100 to 60 V by increasing the quality factor from 276 to 550.

Apart from the Pockels effect, the Quantum Confined Stark Effect (QCSE) creates one of the largest electro-optic coefficients (for TM-polarized light). QCSE is another enabling technology, which is used in telecommunications to design modulators with low power consumption (up to 1 V drive) and fast operation (theoretically at subpicosecond times).[106]

One of the best-performing metasurfaces using this effect has been made of patterned III−V multiple quantum wells.[107] It is designed on a Bragg mirror to ensure near unity reflection in a considered wavelength range. Quantum well consisting of numerous doped semiconductor layers are disposed on top of the mirror and structured into double slits (Figure 3c, top). One of the dips in the reflection spectrum of this structure corresponds to a guided mode (GM) resonance coupled with the high-order multipolar resonance in quantum well grooves. This hybrid GM-multipolar resonance is located close to the wavelength of the interband transition of the quantum well (915−920 nm for this structure). When the DC electric field is applied, QCSE shifts the energy levels and modifies the level of absorption, resulting in a change of a component of a complex dielectric permittivity tensor orthogonal to the layer.[108] Changing the permittivity results in the shift and broadening of a hybrid GM-multipolar resonance (Figure 3c). The second dip in the reflection spectrum in (Figure 3c) corresponds to a hybrid GM-Fabry−Perot resonance, but as it is far from the transition wavelength, it experiences only a negligible modulation. Overall, apart from the high reflection amplitude modulation due to the hybrid GM-multipolar resonance shift (Figure 3c, bottom), the metasurface introduces a phase shift up to 70°. This article also demonstrates a dynamic beam steering with electrical control of isolated metasurface unit elements.

Considerable efforts were already made on the development of miniaturized thin-film electro-optic modulators, and their integration into silicon-based photonic platforms have also been considered.[109−111] These modulators are based on in-plane wave propagation in waveguides, often requiring the structuring of films with standard nanofabrication techniques. In the case of free-space modulators, miniaturization is possible with resonant metasurfaces that require nanostructuring, thus, benefiting from the technology developed for waveguide EO modulators. Patterning EO materials such as lithium niobate require specific etching techniques (such as dry Ar^+ etching) and hard unconventional resists.[110] Apart from etching solid EO materials, coating polymers with organic electro-optic molecules on a nanostructured silicon platform[105] appears even less technologically challenging. Coating metasurfaces with EO materials might nevertheless complicate the pixel-by-pixel addressing issue.

2D Carrier Concentration Modulation. Apart from relying on electro-optic effects, metasurfaces can be tuned electrically by changing the carrier concentration via electric gating. This approach, unlike the EO effects discussed previously, can be used on thin layers of standard CMOS-compatible materials that allow large-scale manufacturing. This method was attempted on various materials such as semiconductors (silicon[112] or indium antimonide[113]) but was especially successful for transparent conductive oxides (TCOs). Carrier concentration in TCOs is considerably smaller than in noble metals, which allows higher changes of the refractive index under applied voltage. However, these changes remain comparatively small with respect to other tuning mechanisms. This problem can be addressed in several ways, which we discuss in the example of one of the most studied TCOs: indium tin oxide (ITO).

A way to increase ITO's optical response modulation is to design ITO-based devices in an epsilon-near-zero (ENZ) regime (close to the point where the real part of the permittivity ε' changes its sign and the imaginary part ε'' is very small).[114−117] While it is hard to reach ENZ in other conductive materials due to high ε'', TCOs can easily reach this regime. Therefore, by changing the position of their plasma frequency while varying the carrier concentration, the larger relative refractive index changes can be introduced. Another approach to further increase tuning consists in summing up the response of several layers using multiple gating.[118,119] Higher modulation can also be reached by using ITO in resonant structures such as a guided-mode resonance mirror,[120] a hybrid plasmonic waveguide mode,[121] or resonant plasmonic antennas.[122] To mention another example of TCO, aluminum−zinc oxide (AZO) was successfully used for the reflection phase and amplitude modulations in a metasurface.[123]

Carrier concentration modulation is also possible in two-dimensional materials, including graphene. Since early works demonstrated tunable and highly confined plasmons in graphene nanostructures,[124,125] there were many attempts to integrate them into electrically tunable metasurfaces operating in a wavelength region from mid-infrared to subterahertz.[126−129] Metasurfaces combining graphene with metallic antennas allow controlling reflection phase and amplitude.[126,130] Although graphene-based metasurfaces for beam-steering and spatial light modulators (SLMs) demonstrate

https://doi.org/10.1021/acsphotonics.1c01833
ACS Photonics XXXX, XXX, XXX−XXX

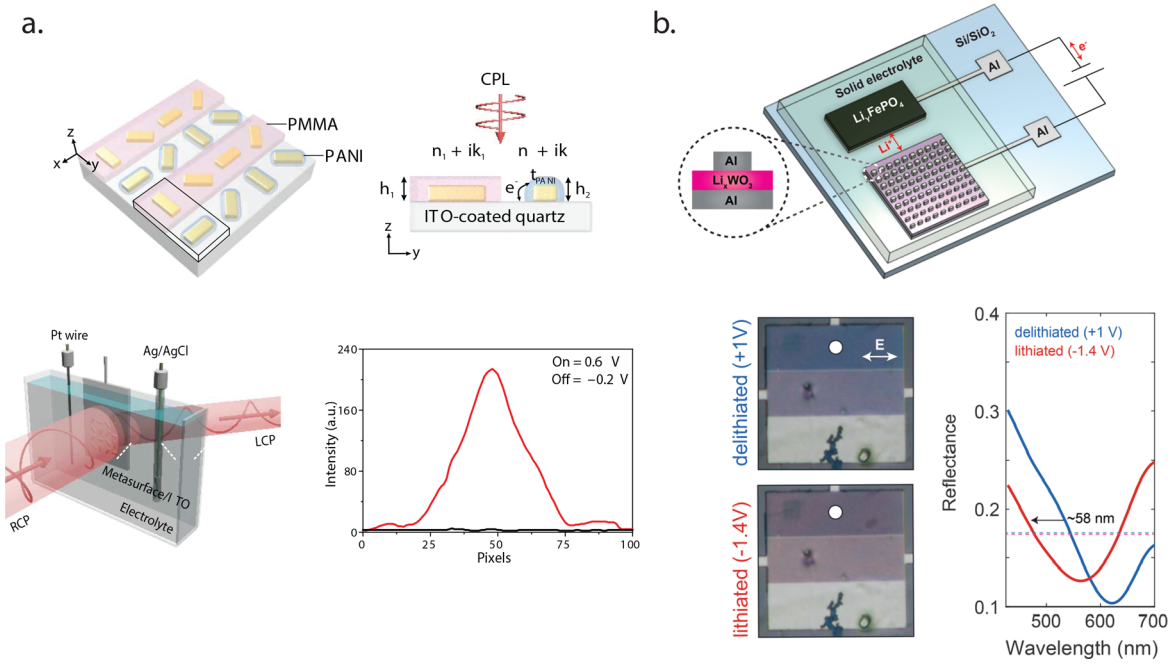

Figure 4. Chemical reactions have been considered for tuning the response of metasurfaces. (a) A beam deflecting the metasurface consisting of plasmonic PB-phase nanostructures is realized by coating every second row of the metastructure with the PANI polymer. The latter changes between the oxidized and reduced form under applied voltage. The figure on the bottom-right shows the reported anomalous transmission intensity contrast. Reprinted with permission from ref 141. Copyright 2021 AAAS; the authors, some rights reserved. Distributed under a CC BY-NC 4.0 license http://creativecommons.org/licenses/by-nc/4.0/. (b) Schematic of WO_3 switchable metasurface by inserting Li^+ ions from a solid-state electrolyte. Lithiated and delithiated spacer in Al/Li_xWO_3/Al particles is used to change the metasurface color, as shown in color-sensitive CMOS camera images. Corresponding reflectivities are shown in the bottom-right panel. Reprinted with permission from ref 145. Copyright 2019 ACS Publications.

sufficiently high phase tuning, their efficiency has to be significantly improved.[131] Another example is tunable perfect absorption in graphene-based metasurfaces[132] which is a promising result for applications requiring photon harvesting.

Despite their low efficiencies, these two modulation schemes reach high switching speeds (up to a few tens of GHz in ITO,[133] for example), making them appropriate for applications requiring fast switching such as LiDAR.[134] The combination of fast tuning mechanisms with optically engineered resonances with high-quality factors, such as quasi-bound states in the continuum, is certainly a meaningful direction to realize ultrathin free-space modulators with a high extinction ratio.

Chemical Reactions for the Realization of Tunable Metasurfaces. Rearranging the constituent of atoms in molecular structures, chemical reactions strongly modify the properties of materials and solutions. Chemical reactions can thus be of interest in adjusting the optical properties of either chemically active metasurfaces or their environments. However, this type of switching appears to be quite slow, typically on the order of seconds or more, which can be reduced to milliseconds by varying unit cell geometry and chemical reaction parameters. Being significantly slower than most of the switching mechanisms considered for fast optical modulation, chemical metasurfaces appear to be an excellent solution for niche applications such as energy-saving smart windows, or flat-panel displays requiring operation frequency of the order of 50−90 Hz.[135] Chemical tuning nevertheless has extremely valuable advantages, including room-temperature operation, low power consumption, and nonvolatile tuning. So far, several mechanisms were proposed for chemically switched devices.

One way to introduce refractive index change of metasurface building blocks relies on a chemical reaction called hydrogenation/dehydrogenation of magnesium (Mg). When interacting with hydrogen, magnesium forms magnesium hydride (MgH_2) through a controlled chemical reaction, that switches the optical properties of the structure from metal to dielectric. By applying oxygen, it is possible to reverse the transition. Considering the reaction time, switching happens within several tens of seconds to several thousands of seconds depending on the sizes of unit cells, the catalytic layer, the hydrogen concentration, and the substrate temperature. Uniform magnesium particles designed for dynamic color displays can be switched from metal to dielectric, thus progressively converting the strong plasmon resonances to weakly interacting dielectric Mie resonances until the scattering colors on the image vanish. Magnesium nanorods inducing the PB-phase were used for tunable phase gradient metasurfaces[136] or for optical signal multiplexing.[137] Applications of this effect include optical information encryption and security. Combined with gold, Mg nanorods were also used to create tunable optical vortices and holograms.[138]

Conductive polymers, such as polyaniline (PANI) polymer, yield another application of chemical switching in the context of metasurfaces. These are bistable low-cost polymers that can be electrochemically switched between oxidized and reduced forms, which induces large variations of its complex refractive index value, in particular, its imaginary part. PANI is particularly interesting for display technology, especially when combined with resonant structures that can provide

https://doi.org/10.1021/acsphotonics.1c01833
ACS Photonics XXXX, XXX, XXX−XXX

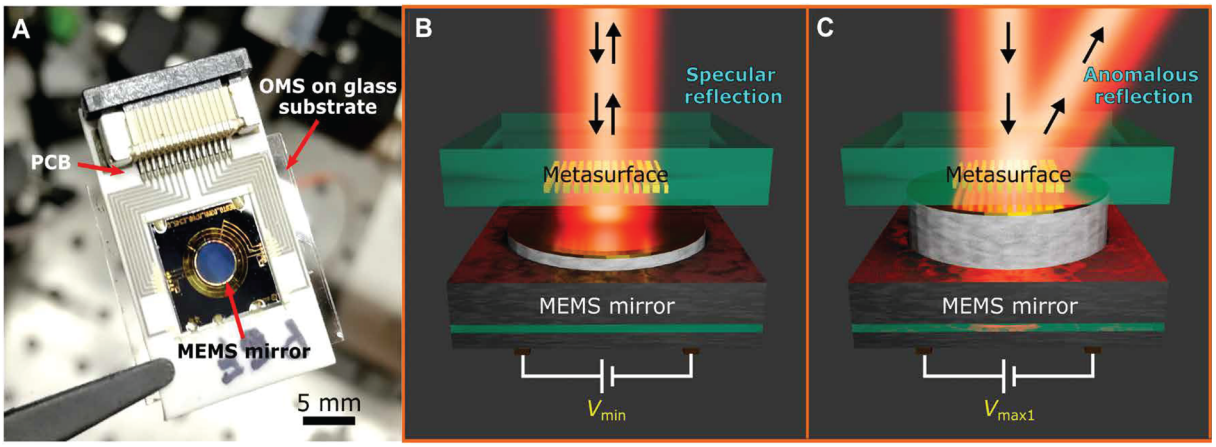

Figure 5. Performance of MEMS-tunable dielectric metasurface lens. (A) Optical platform consisting of MEMS controlled electrically and a gold metasurface placed on top of the mirror on the glass substrate. (B, C) Light impinging on a MEMS-metasurface compound system is manipulated to achieve the desired functionality (deflection) by simply adjusting the distance separating a plasmonic metasurface and a micromirror. Reprinted with permission from ref 153. Copyright 2021 AAAS; the authors, some rights reserved. Distributed under a CC BY-NC 4.0 license http://creativecommons.org/licenses/by-nc/4.0/.

even higher intensity modulation. For example, PANI can be coated on metal nanoslits for tuning the plasmon resonance wavelength,[139] or being used as a shell for plasmonic particles,[140] or even coated on plasmonic particles introducing PB-phase for beam deflection.[141] In particular, alternating coated and noncoated metasurface sections, that is, tunable and not tunable sections, this device produces tunable anomalous transmission with a contrast up to 860:1 (Figure 4a).[141] Phase contrast between the neighboring rows is varied inducing constructive or destructive interference which reveals or suppresses the anomalous transmission intensity. Times to induce and reverse the process are ≈40 and ≈35 ms, respectively. As discussed in the PCM section, cyclability is an important factor to consider when it comes to realistic applications. Current demonstrations reported more than 100 cycle switches. Apart from PANI, other polymers such as poly(3,4-ethylenedioxythiophene)/sulfate (PEDOT/Sulf) polymer network start being investigated for tunable metasurfaces.[142] The advantage of such polymers with respect to other electrochromic materials is that they can be electrodeposited and can create a thin uniform layer with a well-controlled thickness.

The other mechanism of interest for chemical switching of metasurfaces employs inorganic electrochromic materials. The latter has better thermal, chemical stability, and longer durability with respect to organic materials and polymers, and they are compatible with standard physical vapor deposition and lithography processes. However, their switching time is on the order of tens of seconds, limited by ionic diffusion. One of the most popular inorganic electrochromic materials is WO_3, which changes its properties depending on the type of chemical reaction. By Li^+ (or H^+) ion insertion and extraction, it transforms to Li_xWO_3 (or H_xWO_3). It has been used to make several tunable devices such as Bragg-reflector in combination with quantum dots for a tunable luminescent device[143] or core−shell structure combined with TiO_2 for smart-windows applications.[144] CMOS-compatible TiO_2 metasurfaces can be tuned by being exposed to H^+ ions. Another example of the successful implementation of WO_3 for dynamic metasurfaces is shown in ref 145, where it is used as a spacer in a metal−insulator−metal surface producing structural color (Figure 4b). The electrochemical potential of ≈2 V favors lithium insertion that changes its concentration in Li_xWO_3, resulting in a considerable refractive index change of ≈0.3. The device contains a Li_yFePO_4 electrode on Al collector to provide Li^+ ions. This electrode is ionically connected to a metasurface through a transparent solid polymer electrolyte. Applying current to electrodes, the ion-electron interexchange is triggered, which continuously changes the scattered color by the plasmonic structures.

Electrochemical reactions in different electro-chromic materials were previously widely used for large volume commercial applications such as self-darkening mirrors, smart windows, and electronic displays.[146] Reducing the size of these devices down to the nanoscale decreases the switching time. Meanwhile, resonant designs allow the achievement of a full-color palette of interest for the above-mentioned applications.[139] Multiplexed metasurfaces enable polarization-control, further expanding the range of their applications to security and data protection.[137,141]

Pulling, Stretching, and Applying Mechanical Stress for Tuning the Optical Response of Metasurfaces. A promising approach to dynamically address a metasurface functionality is to employ mechanical forces, inducing a relative motion of different parts of the device, stretching, torque, or even movement of a device as a whole.[147] Here we highlight promising works in several conventional mechanical tuning technologies such as microelectromechanical systems (MEMS) and metasurfaces on a flexible substrate. Furthermore, we mention some novel designs such as Kirigami/Origami-based metasurfaces and others. Extensive reviews of active mechanical metasurfaces can be found in refs 148−150.

MEMS-based actuation comprises a popular solution for mechanical metasurface tuning. MEMS devices convert nonmechanical energy inputs to mechanical outputs (i.e., motion, force, torque).[151] MEMS actuators with the highest applicability are the electrostatic, electrothermal, and piezoelectric ones. Electrostatic MEMS actuators have been widely considered for metamaterial tuning.[151] They employ oppositely charged electrodes (a stationary one and a so-called membrane) separated by a tunable distance controlled by the balance between Coulomb and elastic restoring forces to

https://doi.org/10.1021/acsphotonics.1c01833
ACS Photonics XXXX, XXX, XXX−XXX

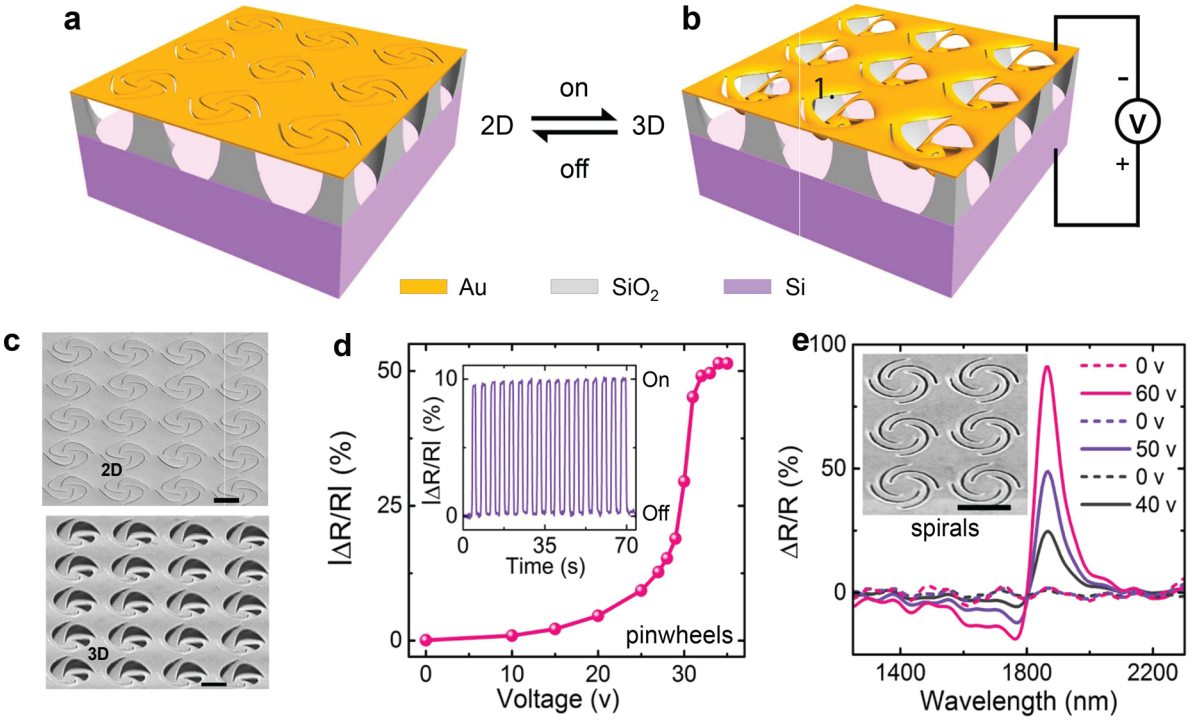

Figure 6. Mechanical tuning of Kirigami-metastructures to modulate the reflection of light. (a, b) Schematic representation of a Kirigami-metasurface. Tuning the geometries of the gold pinwheels from 2D to 3D is realized using electrostatic forces applied between the gold film and the underlying substrate. Downward folding of suspended structures is permitted by underetching a thin layer of SiO_2, creating supporting edge pedestals around the folded elements. (c) Scanning electron microscopy images of fabricated metasurfaces from (a) and (b). (d) Amplitude contrast of the reflectivity at different voltages for a Kirigami-metasurface much larger than the operation wavelength. Inset highlights the on/off reliable cyclability of the reflection amplitude modulation. (e) Response of the resonant Kirigami-metasurface showing a reflection amplitude modulation around a resonant wavelength for different applied voltages. Reprinted with permission from ref 161. Copyright 2021 Springer Nature. Distributed under a CC BY 4.0 license https://creativecommons.org/licenses/by/4.0/.

attract the membrane toward the stationary electrode as a function of the applied voltage. This actuation mechanism is very promising for metasurface tuning since it offers a large range of motion, satisfactory speeds, low power consumption and high compatibility with solid fabrication processes.[152] A possible issue to be considered is the so-called pull-in (or snap-down) effect, corresponding to a critical value in the applied voltage beyond which elastic forces cannot compensate the electrostatic ones, resulting in an unreliable motion. Another actuation approach employs electrothermal MEMS based on layered materials with different thermal expansion coefficients (TEC). Upon the application of electric currents, heat is dissipated through the structure, which expands materials differently according to their TEC. Piezoelectric MEMS have been also proposed for metasurface tuning, mainly due to their low actuation voltage, low power consumption, and high compactness.[153,154] In general, piezoelectric actuators undergo mechanical movements according to the polarity of the applied voltage.[151] Overall, MEMS-based metasurfaces can be triggered to adopt several configurations stemming from vertical and horizontal displacements, or rotational motions of their building blocks. Their actuation speed can reach several kHz and thus it is significantly higher than that of stretchable substrates (~1 Hz). However, here again, pixel-by-pixel MEMS actuation of metasurface building block remains a formidable fabrication challenge, particularly in the visible domain. Several demonstrations concerning the THz and IR regime are reviewed in ref 155.

If pixel-by-pixel control of the meta-atoms is challenging, an accessible solution to integrate MEMS-based metasurfaces in realistic systems consists in tuning the global optical functionalities of the components, sometimes using multistate operation. For instance, we report on the work of Arbabi et al.,[156] where the authors fabricated a MEMS-based varifocal metalens. Their device designed at 915 nm consists of a doublet system, that is, a stationary metalens and a membrane-based metalens. The membrane has mechanical resonances via attractive forces triggered electrostatically. The authors showed that a 40 V actuation results in a kHz micrometric (1 μm) axial displacement of the membrane then causing a ~35 μm shift of the focal distance. Another promising example is a tunable platform composed of a MEMS mirror combined with a plasmonic metasurface (Figure 5).[153] The fabricated device is shown in Figure 5, indicating the MEMS mirror electrically connected through the printed circuit board and the superposed metasurface. The functionalities of this compound system is activated by decreasing the distance between the metasurface and the mirror by applying a relatively small voltage of ≈4 V (Figure 5B,C). An active binary beam deflector with diffraction efficiencies of 40/46% for TE/TM polarization at the 800 nm wavelength has been demonstrated. Broadband operation of 150 nm with a switching speed of ≈2.5 kHz has been realized.

Flexible substrates made of soft materials like low surface energy polymers (for example, polydimethylsiloxane-PDMS) offer multiple advantages for the demonstration of innovative metasurface-based devices with passive or dynamic function-

https://doi.org/10.1021/acsphotonics.1c01833
ACS Photonics XXXX, XXX, XXX−XXX

alities.[157] For instance, their fabrication maturity, low cost, and easy adaptation to surfaces of arbitrary shapes comprise important assets, especially considering the continuous progress of smart wearable devices for AR/VR and medical applications. Programmable contact metalenses with multifocusing capabilities fabricated on curved surfaces to fit the human eye are only one example of the latter. Furthermore, fabricating subwavelength meta-atom arrays on flexible substrates empowers conformal metasurfaces[158] and their related applications, such as cloaking, suitable for real-world implementations.[159] From the point of view of electromagnetic response tunability, elastic substrates allow for controllable and reversible strain deformations under the action of external mechanical stresses. The latter may convert the size and the relative positioning of the meta-units to induce phase discontinuities dynamically. An active metalens comprising gold nanorods has been fabricated on a PDMS substrate for visible operation.[160] Mechanical stretching of the substrate changes the overall curvature of the phase profile produced by the nanoparticles, resulting in a continuous adjustment of the focal length from 150 to 250 μm according to stretching conditions. The authors reported on good reversibility upon sequential stretching−relaxation cycles.

Recently a new concept of optical nano-Kirigami/Origami for tunable mechanical metasurfaces was proposed.[161−163] This mechanism involves bending, cutting, folding, and twisting nanostructures that can be flexibly moved upon external stimuli actuation. One example of nanokirigami has been realized by patterning foldable shapes on a gold film placed above SiO_2 supporting posts (Figure 6a,b, fabricated structures are shown in Figure 6c).[161] By applying an electric field, freely suspended patterns can be bent down, forming 3D structures. Such a design works in two different regimes: a broadband operation is obtained considering the structures as deformable mirrors in the regime when the wavelength is much smaller than unit cells (geometric optics regime), while a narrow band occurs when cutting the patterns to feature optical resonances. In a former case, fabricated structures have a periodicity of 2.5 μm for operation wavelengths band reaching 400−1000 nm, leading to 51% reflection modulation at the central wavelength of 750 nm. The on and off switching requires a comparatively high voltage of 35 V (Figure 6d). In the case of a resonant design, smaller meta-units have a larger stiffness, which requires an even higher actuation voltage of 73 V. However, at resonant wavelength λ = 1860 nm reflection modulation contrast reaches 91% (Figure 6e). In this work, modulation frequency was measured up to 200 kHz and can be subject to further optimization and, according to simulations, can reach up to 10 MHz. Due to their 3D geometries, origami/Kirigami-based structures often possess helicity and chirality, making them extremely interesting for chiral biosensing and detection applications.[164]

Apart from the mechanisms mentioned in this section, several emerging designs with high potential are on the way. For example, cross-stacked nanoparticle chains have been fabricated using colloidal assembly and have been showing large tunable circular dichroism of interest for chiral sensing.[165] Another example is the recently demonstrated meta-vehicle consisting of passive metasurfaces steered along the surface of a fluid using optical forces and torques.[147]

Mechanically actuated meta-optics systems are certainly promising and would participate in further advancing the field of space-time metasurfaces in the coming years. Devices such as MEMS possess a high degree of technological maturity, and they are particularly attractive due to their compatibility with the CMOS manufacturing process and their noticeable modulation performances. For example, thin-film piezoelectric MEMS can achieve up to a 30 MHz modulation frequency,[153] high cyclability (up to 10^{11} cycles at 20 V cycles),[166] and operate at room temperature. Pixel-by-pixel MEMS actuation remains challenging, but solutions to break the structural symmetry in the out-of-plane (third) dimension have been explored in the visible domain, as mentioned above, but also at THz and microwave frequencies.[167] Efforts in addressing individual building blocks at the visible wavelength are nevertheless still needed. Apart from standard technologies, suggested novel designs have a high potential for industrialization due to their mass-production simplicity.[165]

Pushing the Limits of Liquid Crystal Light Modulators toward Active and Adaptive Meta-Optics. Thermotropic liquid crystals (LCs) or, in other words, mesophases appearing between the crystalline solid and the isotropic liquid phase with a temperature change[168] have a long-term tradition in electro-optical devices.[169] Indeed, LCs represent a dominant technology in the display industry, but they have also proven their power in non-display programmable devices such as lenses, spatial light modulators, and beyond.[170] It was inevitable that LCs would attract the interest of the meta-material (-surface) community due to their formidable physical properties, their responsiveness to external perturbations, and their technological maturity. Some relatively early works introducing LCs for metamaterial tuning can be found in refs 171 and 172. Among the different identified LC phases, it is the so-called "nematic" phase that was placed in the foreground for metasurface tunability. Nematic LCs (or NLCs) present strong shape anisotropy at the molecular level leading to long-range orientational order without a translational one. Interestingly, NLCs have orientation-dependent properties such as considerable birefringence (Δn, typically between 0.05 and 0.45), while at the same time they are fluids. NLC average molecular orientation (or "director") is vulnerable to various stimuli including electric and magnetic fields, light, temperature, and mechanical stresses offering large tuning flexibility depending on the targeted application. By reorienting the director with respect to light's **k**-vector, one can select the NLC refractive index experienced by the incident polarized light. To this end, NLCs have been mainly used to dynamically shift the resonances of plasmonic and dielectric metasurface building blocks known to be very sensitive to variations of their optical surrounding. In several demonstrations, an in-plane to out-of-plane switching is used, where the angle between the director and the light's wavevector defines the refractive index and leads to electrically controlled birefringence (ECB). It holds that $n_e(\theta) = \frac{n_e n_o}{\sqrt{n_e^2 \cos^2\theta + n_o^2 \sin^2\theta}}$, where n_e is the extraordinary refractive index, n_o is the ordinary one, θ is the angle between the director and the light's **k**-vector, and $\Delta n(\theta) = n_e(\theta) - n_o$ is the ECB. These equations show that NLCs can be used for both binary on−off switching, but also to induce continuous refractive index gradients. The latter constitutes the basis of NLC-SLMs operation.[173] Electrically triggered NLC metasurfaces have been also used to control the polarization of the light in twisted-nematic cells known to induce optical activity.[174] For any NLC alignment, when the voltage is sufficiently increased, a NLC with a positive (negative) dielectric anisotropy will tilt along

https://doi.org/10.1021/acsphotonics.1c01833
ACS Photonics XXXX, XXX, XXX−XXX

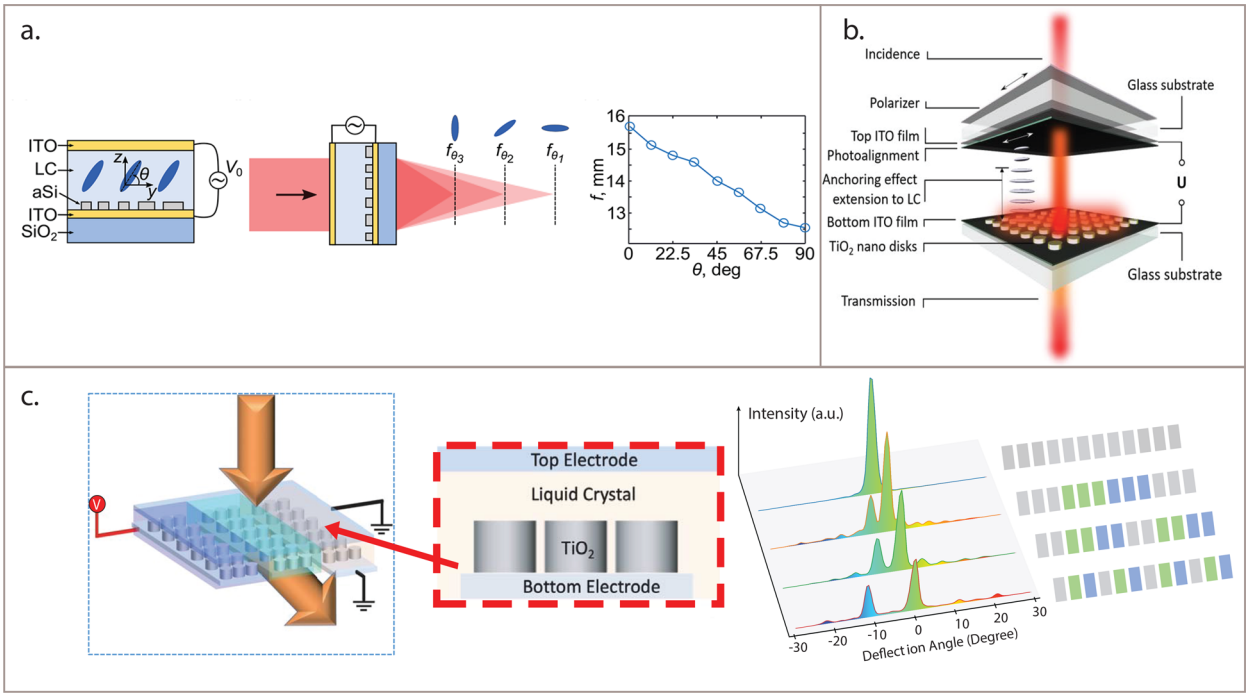

Figure 7. Tunable metasurfaces infiltrated with liquid crystal molecules. (a) Si-based metalens encapsulated with NLC. By changing the LC reorientation angle electrically, a varifocal function has been demonstrated. Reprinted with permission from ref 177. Copyright 2021 ACS Publications. (b) Electrically addressable transmissive device based on TiO_2 metasurface infiltrated with an NLC. At the V_{OFF} state, the NLC is aligned along the photoalignment direction imposed at the cover window. Asymmetric alignment is established at the different cell sides. Due to the strongest anchoring at the metasurface side, the bottom alignment condition is dominant in the cell. Adapted with permission from ref 186. Copyright 2019 Nature Publishing Group. Distributed under a CC BY 4.0 license https://creativecommons.org/licenses/by/4.0/. (c) Phase-only SLM in transmission based on a TiO_2 metasurface tuned by a NLC. The device is composed of pixelated bottom electrodes each having three TiO_2 nanopillars on the top. A common upper electrode is considered for the voltage application. The device is infiltrated with a NLC tuned at three voltage levels (blue−green−gray) along the sequential electrodes to deflect the incident beam. A maximum deflection angle of 11° has been demonstrated. Adapted with permission from ref 178. Copyright 2019 AAAS; permission conveyed through CCC, Inc.

(perpendicular) the electric field's direction so as to minimize its free energy. The mechanism behind the electrically induced NLC reorientation involves the competition between electric, elastic, and anchoring forces. The latter describes the formation of a specific director's orientation at the interfaces between the LC and solid substrates that confine the anisotropic fluid in practical applications. We highlight here that NLCs are very attractive to metasurfaces since they respond to few volts (usually 1−5 V), they possess broadband birefringence, as well as they present small or negligible losses in wide spectral windows. An all-optical metasurface tuning has also been successfully demonstrated showing the versatility of NLC responsiveness.[175,176] It is interesting that the NLC's fluid nature allows a straightforward infiltration into prefabricated passive metasurfaces serving at reducing costs and complexity.

Independently of the employed stimulus, NLC addressable metasurfaces have already shown their large potential for several applications, including varifocal metalenses (see for instance Figure 7a),[177] spatial light modulators,[178] projection displays,[179,180] sensors,[181] thermal camouflage,[182] and so on. Moreover, devices operating at different spectral regions show the flexibility in adapting conceptualized operation principles at different frequencies ranging from microwaves to visible.[178,183−185] However, except for the obvious advantages, there are still reported constraints that need to be tackled. We find it useful to direct the following discussion toward two axes that have to be carefully considered for the realization of NLC-tunable metasurfaces. These are the control of NLC alignment at the metasurface vicinity and the improvement of the NLC response time in the case of electrical tuning.

Uniform NLC alignment before the application of any perturbation is critical in LC-based applications since it ensures a high degree of order that maximizes the optical anisotropy. NLC anchoring conditions at the interfaces with other materials is very sensitive to the NLC properties as well as to the chemical composition and the structure of the underlying surface. In LC displays, the anisotropic fluid is confined between glass substrates covered with transparent electrodes and alignment layers. The existence of such layers ensures a uniform director's field before the voltage application. Alignment coatings are usually created by either mechanical rubbing or photoalignment. However, when the NLC is infiltrated into a subwavelength structured environment, such as a metasurface, imposing a particular alignment condition is not a trivial task. Several groups have reported on the issue of NLC's poor alignment close to metasurfaces, while others adopted strategies to prevent or eliminate this issue. Sun et al. discussed the importance of the anchoring condition of the NLC mixture E7 at the vicinity of a TiO_2 dielectric MS composed of 190 nm thick cylindrical structures (Figure 7b).[186] In that work, a 1.5 μm thick E7 cell is sandwiched between the metasurface fabricated on the top of an ITO layer and a top window covered with a second electrode. Then a voltage application causes bulk NLC reorientation to modify the refractive index and thus tune the metasurface resonances.

https://doi.org/10.1021/acsphotonics.1c01833
ACS Photonics XXXX, XXX, XXX−XXX

To ensure the uniform in-plane orientation of the NLC molecules at the V_{OFF} state, the authors use photoalignment for the cover window. However, they found that there is a deviation angle between NLC alignment close to the metasurface and the photoalignment direction. By considering the NLC free energy expansion and using an Euler−Lagrange minimization process, they explained that the anchoring condition close to the meta-structures is strong enough to dominate over the photoalignment direction. An even more decisive alignment strategy has been suggested by Su et al.[187] that encompasses mechanical rubbing at the upper window and photoalignment treatment at the bottom metasurface. Nevertheless, the authors highlighted the importance of the metasurface topography upon the NLC molecules orientation close to the meta-atoms. In their recent publication, Lininger et al. presented experimental results showing the impact of NLC director inhomogeneities on the optical response of infiltrated metalenses.[188] Dolan et al. discussed the effect of NLC radial disordering around cylindrical pillars on the optical near fields of TiO_2 metasurfaces in the visible range and proposed numerical simulation strategies for accounting for these phenomena.[189] They, among others, emphasized the emergency of optically simulating the NLC via its dielectric permittivity tensor, especially when the disorder is present close to the metasurface building blocks. In the latter publication, vertical alignment of the NLC molecules has been considered by chemical functionalization of the metasurface and the upper window by octadecyltrichlorosilane (ODTS) in heptane solution. Chemical treatment seems to reduce the complexity in terms of fabrication compared to mechanical rubbing and photoalignment since it may be applied to the metasurface as a postfabrication process. Moreover, it can be employed to control the anchoring strength of the NLC layer immediately adjacent to the metasurface, accounting also for the metasurface fragility. In the presence of very strong anchoring, the NLC molecules at the near-field of the meta-units will not respond to the external field. This issue can be controlled by relaxing the anchoring forces close to the metasurface.[190] The reduction of the metasurface substrate contribution has also been proposed as a solution to moderate anchoring forces close to the meta-atoms.[191] The NLC director is very sensitive to the geometries of other materials placed in its vicinity. Generally, it is anticipated that structures generating an anisotropic environment compatible with the NLC molecular shape will lead to enhanced alignment. For instance, grating-like metasurfaces could be an alternative[192] compared to cylindrical pillars generally reported to be associated with local NLC disorder.[192] Finally, high aspect ratio structures have been proposed for NLC vertical alignment.[193]

The use of NLC metasurfaces for realistic applications requiring ultrafast, real-time tunability is a great challenge. For instance, beam steering devices that could be used as laser scanners for LiDAR systems require scanning frequencies on the order of MHz. Electro-optical devices based on NLCs are known to exhibit millisecond switch-on (τ_{ON}) and relaxation (τ_{OFF}) responses ($\tau_{ON} < \tau_{OFF}$). kHz speed is adequate for display applications due to the human eye's perception capabilities, but it is too slow for more demanding applications, including LiDAR scanning. NLC voltage-response time is dictated by the intrinsic physical properties of the employed molecules (i.e., the elastic constants, the rotational viscosity, and the dielectric anisotropy), as well as by the temperature, the anchoring strength, and the distance between the electrodes. For a given NLC molecule, the switching time is proportional to the square of the distance between the electrodes. Typical phase-only LC-SLM devices employ planar electrodes confining a NLC layer. The top electrode usually acts as a reference, while the bottom one is pixelated to induce a gradual 2π phase retardation to the process of light propagation. Since the phase retardation is exclusively accumulated into the NLC layer, the distance between the electrodes is at least a few microns for visible wavelengths and typical Δn values. Moreover, these conventional SLMs targeting visible applications are fabricated with a micrometric pixel pitch that leads to low deflection angles, multiple diffracted orders, and reduced efficiency. In their work, Li et al. reported on uncoupling the phase modulation from NLC thickness by using a Huygens dielectric metasurface, where the main phase accumulation happened inside the TiO_2 nanopillars.[179] The latter is of particular interest not only for faster beam steering but also for moderating pixel crosstalks, unavoidable in bulky LC cells. The authors demonstrated a NLC metasurface beam steering device in the visible range with a maximum deflection angle of 11° and 36% efficiency in transmission (Figure 7c.). Other reported approaches for enhancing both τ_{ON} and τ_{OFF} have proposed dual-frequency LCs known to change the sign of their dielectric anisotropy according to the frequency of the applied electric signal.[194] A particularly promising approach for speeding up the LC response time has been proposed in a recently released patent introducing LC metasurfaces operating in the reflection mode as a valuable solution for ultracompact LiDAR systems.[195] In this patent, the authors propose the employment of metallic vertical (instead of planar) electrodes to electrically activate the LC infiltrated between them in a tiny (subwavelength) volume. The electrode distance reduction speeds up the LC response time to a few tens of microseconds. Interdigital electrodes have also been discussed in the recent past as a solution for achieving submillisecond responses.[192] However, by also extending the height of the electrodes over the whole device thickness, one enhances electric field uniformity and eliminates interpixel crosstalks in pixelated programmable metasurfaces.

Finally, we are questioning if the maturity of LC technology is enough to follow the continuously increasing demands of tunable metasurface applications? As explained in the previous paragraphs, the principal reported challenges in LC-metasurface technology are dealing with the ability to control the alignment properties at the metasurface environment and to enhance the NLC time-responses. The recent advances revealed that these problems can be tackled by reconsidering novel device architectures with dedicated alignment procedures. To that end, we believe that the strong industrial activities around LC electro-optical devices would help LC-tuned metasurfaces to access the market faster than the other solutions discussed in this report. However, we highlight that efforts are needed not only from the metasurface but also from the LC scientific community. For instance, novel NLC molecules with improved physical properties and LC phases beyond nematic (smectic and blue phases) could be investigated to further improve their integration with metasurfaces. The employment of ferroelectric LC phases known to exhibit microsecond responses could be an alternative for fast switching.[196]

https://doi.org/10.1021/acsphotonics.1c01833
ACS Photonics XXXX, XXX, XXX−XXX

Table 2. Table Comparing Five Selected Tuning Mechanisms Considering Their Advantages and Bottlenecks and Highlighting Examples of Possible Applications

Tuning mechanism	Illustration	Advantages	Bottlenecks	Applications
PCM	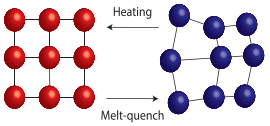	• Large Δn • non-volatile Chalcogenide PCM • material options with low losses • multi-state operation • high/ medium cyclability • fast switching: up to kHz for metasurfaces (10 kHz in[90] for GST), up to 10 MHz for optical memory[198]	• non-uniform heating • cooling that limits switching speed • High losses in VIS and NIR for GST	• non-resonant components for broadband applications due to large Δn • fast-speed application for optimized structures • Non-volatility enables optical neuromorphic applications[199]
Electro-optic effect	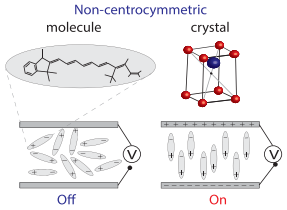	• Fast switching (up to 5 GHz)[105] • Low power consumption • High cyclability • High transparency in VIS	• Small index change	• High-speed communication and computing
Chemical tuning	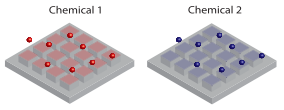	• Cheap/facile to fabricate polymers • Bi-stability • Low power consumption ($\approx 1V$) • Continuous tuning • room temperature operation	• Slow switching ($\approx 10ms - 1000s$)	• Slow modulation applications including electronic displays and smart windows • Security and data protection[137,141]
Mechanical tuning	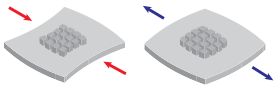	• Optical contrast provided by geometry tuning • Fast switching (up to 100 kHz) • Power consumption can be less than 20 mV • MEMS- and CMOS-compatible	• Difficulty of scaling down • Low lifetime for stretchable substrate • Constraint imposed by moving parts	• Switchable lenses or deflectors for free-space optical tracking /communication[153] • Chiral sensing[165] • Spectral modulation[200]
Liquid Crystals	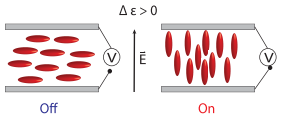	• High transparency in several spectral regimes including VIS • Straightforward infiltration due to fluid nature • Low-cost materials • Low power consumption • response at low voltages $\approx 1 - 5V$ • ON-OFF and continuous tuning • room temperature operation • Highly mature technology	• polarization dependency • sensitivity to MS topography • slow switching in bulk devices	• Displays • Next generation of compact LiDARs[195] • Fast optical interconnects

https://doi.org/10.1021/acsphotonics.1c01833
ACS Photonics XXXX, XXX, XXX−XXX

PERSPECTIVES

In this Perspective, we selected among the most promising approaches reported so far for applications requiring real-time and programmable light manipulation with planar metasurfaces. Our selection criteria encompass the level of readiness of the technology to penetrate the industrial market, the complexity in terms of design and fabrication, the reported performances, and the device reliability. Up to now, research efforts devoted to metasurface tunability mainly propose materials that adapt their optical properties to external agents, including electric fields, light, temperature, and mechanical forces. These materials can be used either for subwavelength building blocks or the tunable optical environment for intrinsically passive meta-units. The various mechanisms for metasurface tuning that have been demonstrated exhibit different performances and properties. Therefore, one can select among the different available mechanisms according to the targeted application or equivalently to the performance. As an example, electro-optic materials are good candidates for hybrid photonics complementing silicon-based platforms due to exceptionally high modulation frequencies typical for these materials, generally in the GHz regime.[109] NLC and chemically tunable metasurfaces are more promising for display applications due to their low-voltage operation, relatively low addressing speed, and comparatively low cost. More application possibilities are summarized in Table 2 by considering the individual advantages of each tuning mechanism. Interestingly, the apparent limitations of a given modulation mechanism can be turned into significant advantages. For example, the extremely large optical losses of GST material could be utilized for applications requiring fast programmable amplitude modulation.

If current efforts on tunable metasurfaces concern mainly academic research, the continuously growing industrial interest for dynamic, ultracompact, and integrated optical components demands the quick laboratory-to-market transition. The synergy between different scientific and technological disciplines spanning physics, chemistry, nanotechnology, electrical engineering, and computer science is the key to speeding up the process for bringing dynamic metasurfaces ready to market applications. CMOS (complementary metal oxide semiconductor) technology, being the cornerstone for manufacturing micro- and nanodevices, is considered for the mass production of dynamic metasurfaces, such as the Lumotive example that cofabricated LC metasurfaces with a Himax semiconductor specialist. ST microelectronics, a world leader in MEMS and PCM memory industrialization, could play a significant role in the industrialization of PCM metasurfaces. Electrical tuning (which is clearly the most promising and most practical modulation technique) architectures remain complex, requiring pixel-by-pixel voltage application bridging subwavelength features with a large-scale electronic driving board. Commercially available display drivers exploiting the similarity with the highly mature LCD technology would be useful for speeding up the market readiness of LC actuated metasurfaces, but customization of the electronic architectures to enable individual control of the meta-atoms by field-programmable gate arrays (FPGA) is inevitable. The development of advanced algorithms to program the designed optical functionalities in real-time is still needed. These algorithms are of interest to perform dynamic postfabrication optimization aiming at maximizing the performance of tunable metasurfaces. Postprocess optimization is generally not achievable with passive metasurface counterparts. In their recent review, Tsilipakos et al.[197] discuss the possibility of software-defined metasurface networks that enable intracommunication as well as an interaction with the external environment by user-friendly interfaced applications. Systems embedding one or several metasurfaces will thus be considered in the future for various applications consistent with the terms IoT and AoT.

Addressing not only fast but ultrafast light modulation, on the order of a fraction of the optical frequency, offers new interesting academic perspectives in particular with the emerging topic of space-time metasurfaces. Spatiotemporal control of electromagnetic waves extends the realm of functionalities enabled by the conventional tuning mechanisms explicitly discussed above. In particular, breaking time-reversal symmetry might be interesting for the realization of a new class of nonreciprocal optical systems. A discussion explaining the physical mechanisms and solutions currently studied at the academic level, including the use of bianisotropic metasurfaces is provided.

In the Introduction, we mentioned that the foundation of optical metasurfaces obeying the generalized laws of reflection and refraction[17] consists in modifying the tangential momentum of light upon reflection and transmission. New degrees of freedom leading to broader versions of these laws can be induced by considering the temporal dependency of these phase gradients.[201] Space-gradient-only metasurfaces are restricted by Lorentz reciprocity and are thus called reciprocal. A system is defined as reciprocal when the ratio of the received to the transmitted field is not changing as one exchanges the transmitter and the receiver.[202,203] Usually, reciprocity is defined by symmetry in the electromagnetic trajectory upon time-reversal. Time-reversal symmetry is thus equivalent to reciprocity when (1) the trajectory corresponding to the original forward process coincides with the time-reversed trajectory and (2) the absolute amplitude of the originally transmitted field is equal to the amplitude of the received field upon time-reversal. For a loss- (gain-) less system (1) and (2) both guarantee reciprocity and time reversal symmetry. However, in a lossy system time-reversal symmetry is broken due to the violation of (2). For instance, as light travels through a lossy metasurface, its amplitude decreases, and as it travels back in a time-reversed scenario, it decreases even more but by the same percentage. This metasurface is reciprocal because the ratio of the received to the transmitted field is the same for forward and backward propagation directions (symmetry in terms of field ratios), but the time-reversal symmetry is broken because the absolute field amplitudes are different (asymmetry in terms of absolute fields).[203] Very good and comprehensive tutorials discussing in detail the different aspects of time-reversal symmetry breaking and other notions concerning the reciprocity concept are available in the literature.[203−207]

Breaking reciprocity for electromagnetic waves would mean realizing components such as diodes, optical isolators, and circulators, that is, devices generally providing asymmetric responses.[208] However, using a structurally asymmetric device would not be sufficient for nonreciprocal devices since time-reversal symmetry should also be broken. The conventional way to break time-reversal symmetry encompasses the employment of magnetic materials triggered by internal or external magnetic fields. However, these materials exhibit limited applicability, especially at optical frequencies stemming

https://doi.org/10.1021/acsphotonics.1c01833
ACS Photonics XXXX, XXX, XXX−XXX

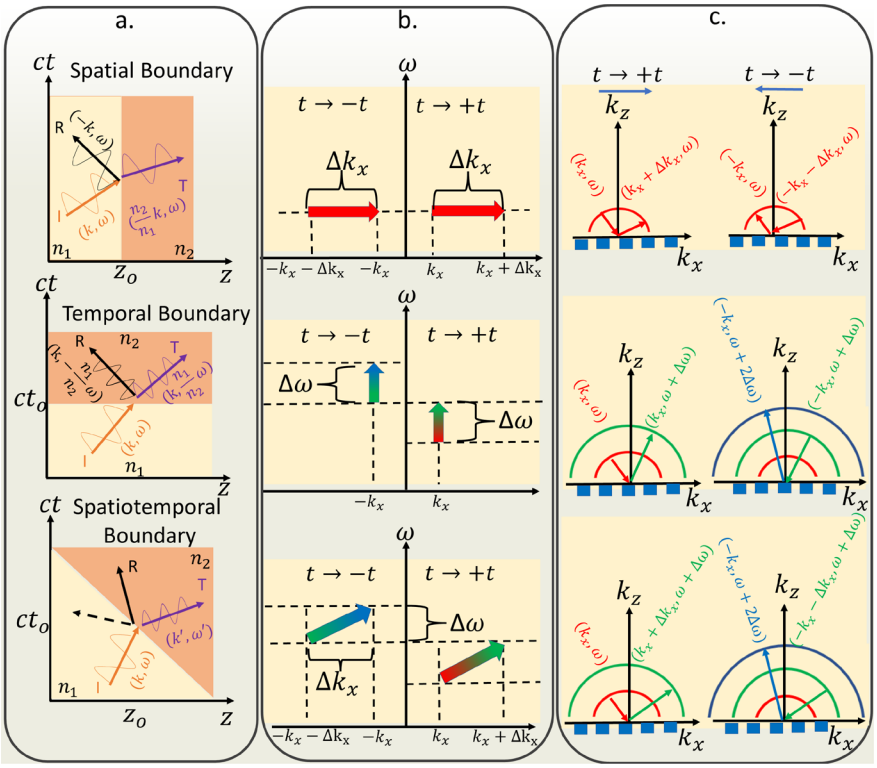

Figure 8. (a) Top to bottom panels illustrate the wave scattering process from a spatial, a temporal, or a spatiotemporal boundary separating two media of refractive indices n_1 and n_2, respectively. In all the panels, I, R, and T hold for the incident, reflected, and transmitted waves, represented then as orange, black, and purple arrows, respectively. The incident wave always has a momentum k and a frequency equal to ω. (b, c) An example showing a space-, time-, and space−time-modulated reflective metasurface (from top to bottom in both b and c). In particular, (b) presents the frequency and the tangential momentum transitions upon reflection for both forward ($t \to +t$) and time-reversed ($t \to -t$) propagation. A space-gradient along the x-direction is considered in (b), top and bottom panel, providing an extra tangential momentum $\Delta k_x > 0$ for both $t \to +t$ and $t \to -t$, thus, adding (subtracting) Δk_x upon forward (time-reversed) propagation. The temporal modulation in the middle and the bottom panel up-converts frequency for both $t \to +t$ and $t \to -t$ cases. The solid-filled red arrow in (b), top panel, represents the horizontal momentum transitions without frequency change for space-gradient only. The gradient-filled arrows in (b), middle and bottom panels, show that the vertical and the oblique transitions for temporal and spatiotemporal modulation are accompanied by a frequency shift without or with a tangential momentum change, respectively. (c) $t \to +t$ and $t \to -t$ trajectories of a wave interacting with a spatially (top), temporally (middle), and spatiotemporally (bottom) modulated reflective metasurface. The red, green, and blue semicircles represent the isofrequency curves corresponding to ω, $\omega + \Delta\omega$, and $\omega + 2\Delta\omega$, respectively. The blue arrows on top of the figures indicate the later forward and the later time-reversed wave. Clearly, panel (a) corresponds to a (non)reciprocal response.

among others from their bulkiness, losses, cost, and integration inconvenience. Magnetic-free approaches are therefore highly desirable for opening the way for the demonstration of nonreciprocal components.

Nonlinear metasurfaces have also been proposed as magnetic-free solutions to break reciprocity.[209] These materials present optical responses that are dependent on the applied electric field intensity. In particular, the proportionality of the coefficients between the polarization of the nonlinear field terms are the high-order susceptibility tensors leading, according to their order, to prominent nonlinear effects such as the Kerr effect, second (third) harmonic generation, SHG (THG), and so on. Nonlinear metasurfaces require very high light intensities that are not always desirable in practical applications due to inconvenient power requirements.

During the last years, the focus on breaking time-reversal symmetry accompanied by multiple-harmonic generation was concentrated around the temporal modulation of different metasurface properties. One of the pioneering works introducing space-time metasurfaces is that of Hadad et al.[210] To this end, several other efforts have been dedicated to the conceptualization and the demonstration of time-varying metasurfaces.[211−213] In practice, controlling the metasurface functionalities in time is not an easy task, especially when considering ultrafast modulators. This can be achieved in the microwave regime, for instance, by employing varactor and PIN (positive-intrinsic-negative) diodes. Just to mention some interesting concepts and demonstrations, Zhang et al. proposed space-time-coding metasurfaces to isolate reflections in the space and the frequency domain, controlled by a PIN diode programmed by digital codes.[214] They experimentally verified nonreciprocity in the frequency domain. Liu et al. suggested a time-varying Huygen's metasurface for parametric wave scattering at microwaves using varactor diodes as tunable elements.[215] The authors supported their concept by experimental results and, among others, claimed that their idea could be brought at optical frequencies by exploiting modulation mechanisms such as electro-optic and acousto-optic effects. Very recently, the concept of a nonreciprocal electromagnetic isolator has been presented, supported by numerical results introducing a space-time coding metasurface based on electronic rotational Doppler shifts.[216] In Figure 8 we provide a simplified illustrative example presenting wave-engineering capabilities achieved by space-only, time-only, and

https://doi.org/10.1021/acsphotonics.1c01833
ACS Photonics XXXX, XXX, XXX−XXX

space-time discontinuities. Figure 8a presents the general wave-scattering process of an incoming plane wave (I) $\vec{E}^{I}(\vec{r},t) = \vec{A}e^{i(\vec{k}\vec{r}-\omega t)} = \vec{A}e^{i\phi(\vec{r},t)}$, where $A = |\vec{A}|$ is the amplitude and $\phi(\vec{r},t)$ is the phase when it encounters spatial, temporal, and spatiotemporal discontinuities in the optical density of a medium. The phase depends on both spatial and temporal coordinates, where $k = |\vec{k}|$ is the wavenumber composed of a transverse momentum $k_{\parallel} = k_x$ and ω is the frequency. In particular, as progressively illustrated in Figure 8a from the top to the bottom, the incident wave impinges on a spatial, temporal, and spatiotemporal boundary separating two different optical media of refractive index n_1 and n_2, respectively. In the space scenario, the boundary is placed at a particular position z_o of the space coordinate axis, where n_1 corresponds to $z < z_o$ and n_2 to $z > z_o$. In such a case, the incident wave (represented by an orange arrow) will be partially reflected back in the medium n_1 (black arrow, R holds for reflection) and partially refracted in the medium n_2 (purple arrow, T holds for transmission), as described by Snell's law. Crossing the spatial boundary, the beam will not change its frequency due to energy conservation. However, the total momentum changes to account for the refractive index change given the dispersion relation $k = \frac{\omega}{c}n$, where c is the speed of light in a vacuum. The momentum in the second medium is equal to $k_2 = \frac{n_2}{n_1}k$, where k is the incident wavenumber, while the reflected wave is propagating along $-k$. In the temporal scenario, the refractive index changes from n_1 to n_2 at a particular moment in time and for all the positions in space, which is equivalent to splitting two media with refractive indices n_1 and n_2 at a temporal interface t_o. As illustrated in Figure 8a, the middle panel for $t < t_o$, the refractive index is n_1, and for $t > t_o$ it is n_2. A wave traveling in the $t < t_o$ regime is an earlier wave compared to the later waves occurring for $t > t_o$. In this scenario the momentum carried from the light traveling forward in the medium n_2 (purple arrow) is conserved, but the energy is not. The second panel of Figure 8a describes what is called "time refraction", and it can be perceived as the temporal counterpart of the conventional Snell's law leading to the frequency shift of the refracted beam. A wave traveling later backward in time, imposing a time-reversed scenario where $t \rightarrow -t$ holds for the time reflected wave (black arrow). Note that the absolute value of the frequency change of the transmitted and the reflected waves in the second medium $\left(|\omega_2| = \frac{n_1}{n_2}\omega\right)$ is the same for both waves, as it depends only on the optical densities of the two media. In Figure 8a (middle), we denote the time-reversed reflected (R) wave with a negative sign in front of the frequency to indicate that the propagation occurs in the later backward direction in time. The bottom panel in Figure 8a corresponds to the general case where a spatiotemporal boundary separates the two media n_1 and n_2. A wave crossing such a boundary will change both its frequency and its momentum, as indicated by (k', ω'). The two black arrows in Figure 8a, bottom panel, show that the reflected beam can propagate either in the medium n_1 (dashed arrow) or in the medium n_2 (solid arrow), depending on the velocity of the interface. In particular, if the interface moves slower than the speed of the light (subluminal case), the wave will be reflected inside the medium n_1, while it will be reflected inside the medium n_2 when the velocity exceeds c (superluminal case).[206,217]

After introducing the different spatiotemporal boundaries, we could now discuss cases of time-modulated nanostructured interfaces, leading to Doppler-like frequency conversions, breaking both time reversal symmetry and reciprocity, as introduced in ref 201. Let us consider the case of a metasurface that induces phase discontinuities on reflected and transmitted fields. Here, we consider reflection only in an optical medium n for simplicity. These phase discontinuities we are considering hereafter can be induced in space and time over a fixed spatial period along the x-direction with a uniform temporal modulation, that is, considering only the same frequency modulation for all the elements of the period. For an obliquely injected plane wave at the metasurface, $\phi(\vec{r},t)$ is representing the spatial and the temporal phase evolution. Its frequency can thus be written as $\omega = -\frac{\partial\phi(\vec{r},t)}{\partial t}$ and its transverse wave vector along the x-direction as $\vec{k}_x = \left(\frac{\partial\phi(\vec{r},t)}{\partial x}\right)\hat{x}$. Spatiotemporal modulation adds an extra tangential momentum $\Delta k_x = \frac{d\phi(x,t)}{dx}$ and shifts the frequency of the incident wave by a factor $\Delta\omega = -\frac{d\phi(x,t)}{dt}$. Under such a consideration, the phase of the reflected wave can be expressed in terms of its wavenumber and its frequency is given by

$$k_{R,x} = k_{I,x} + \Delta k_x \Rightarrow k_R \sin\theta_{R,t\rightarrow+t} = k_I \sin\theta_{I,t\rightarrow+t} + \Delta k_x \quad (1)$$

$$\omega_R = \omega_I + \Delta\omega = \omega + \Delta\omega \quad (2)$$

In eqs 1 and 2, the subscripts I and R correspond to the incident and the reflected wave, respectively, while the notation $t \rightarrow +t$ shows that the time moves forward. Combining eq 2 with the dispersion relation $k = \frac{\omega}{c}n$, we have

$$k_R = \frac{n}{c}(\omega + \Delta\omega) \quad (3)$$

Due to eq 3, eq 1 brings the spatiotemporal version of the generalized law of reflection, written as

$$\sin\theta_{R,t\rightarrow+t} = \frac{\omega}{\omega + \Delta\omega}\sin\theta_{I,t\rightarrow+t} + \frac{c}{n(\omega + \Delta\omega)}\Delta k_x \quad (4)$$

Similarly, we derived the generalized space-time Snell's law, leading to

$$\sin\theta_{T,t\rightarrow+t} = \frac{n\omega}{n_2(\omega + \Delta\omega)}\sin\theta_{I,t\rightarrow+t} + \frac{c}{n_2(\omega + \Delta\omega)}\Delta k_x \quad (5)$$

The subscript T in eq 5 refers to the transmitted wave, while n and n_2 are the refractive indices of the incident and the transmitted medium, respectively.

Now we consider the reflection cases of space gradient and time modulated metasurfaces independently.

Space-only modulated metasurface: for a pure space gradient ($\Delta k_x \neq 0$), we substitute $\Delta\omega = 0$ in eq 4 to get:

$$\sin\theta_{R,t\rightarrow+t} = \sin\theta_{I,t\rightarrow+t} + \frac{\lambda}{2\pi n}\Delta k_x \quad (6)$$

As expected, eq 6 describes the generalized law of reflection,[17] where λ is the free-space wavelength. Now let us suppose that a wave is impinging on the space-only gradient metasurface at an angle $\theta_{I,t\rightarrow-t} = \theta_{R,t\rightarrow+t}$, mimicking a time-reversed scenario where $t \rightarrow -t$, as in practice time, cannot be reversed. In such a case, $\phi(x)$ is constant in time and $\Delta\omega = 0$.

https://doi.org/10.1021/acsphotonics.1c01833
ACS Photonics XXXX, XXX, XXX−XXX

Substituting $\Delta\omega = 0$ in eq 4 and replacing $\theta_{I,t\to+t}$ by the time-reversed incident angle $\theta_{I,t\to-t} = \theta_{R,t\to+t}$, we find that the reflected wave in the time-reversed scenario leaves the metasurface at an angle $\theta_{R,t\to-t} = \theta_{I,t\to+t}$, subtracting thus a tangential momentum Δk_x from the incident wave. To summarize, in the time-backward process, the reflected beam from a spatial only modulated interface reflects at the same angle as its conjugate ($t \to +t$) in the time-forward process, which is the definition of reciprocity in lossless systems. The process is illustrated schematically in the top panels in Figure 8b and c. In particular, in Figure 8b, the process is represented by horizontal wavenumber transitions in the (k_x, ω) space for both $t \to +t$ and $t \to -t$, resulting from the energy conservation restriction for space-only modulated metasurfaces.

Time-only modulated metasurface: we call the time-only modulated metasurface an interface patterned with an array of homogeneous nanostructures that are all modulated similarly in the time domain where $\Delta k_x = 0$ and $\Delta\omega \neq 0$. Equation 4 requires studying both time-forward and time-backward cases separately. First, we examine the time-forward scenario ($t \to +t$), where the incident wave is impinging on the metasurface at an angle $\theta_{I,t\to+t}$ and it is reflected at angle $\theta_{R,t\to+t}$, calculated given the frequency shift (Figure 8c, middle panel, left) and given by

$$\sin\theta_{R,t\to+t} = \frac{\omega}{\omega + \Delta\omega}\sin\theta_{I,t\to+t} \tag{7}$$

Now let us suppose the time-reversed scenario ($t \to -t$), with an incident wave impinging on the metasurface at an angle $\theta_{I,t\to-t}$. As shown by the vertical transitions, arrows in Figure 8, middle panel (left), in the case of time-gradient, the metasurface is modulated to add an extra frequency shift, $\Delta\omega$, also during the time-reversed process.[214] Such frequency conversions are equivalent to Doppler shifts. In particular, a Doppler shift can occur when we consider either that the object is moving relative to the source or similarly that it is stationary but its refractive index varies in time. This frequency conversion is also consistent with energy nonconservation, where a frequency shift is responsible for energy transfer $\Delta E = \hbar\Delta\omega$. We substitute $\frac{\omega}{\omega+\Delta\omega}$ in eq 7 with its time-reversed counterpart $\frac{\omega+\Delta\omega}{\omega+2\Delta\omega}$, leading to a reflected angle $\theta_{R,t\to-t} \neq \theta_{I,t\to+t}$. That is, the time-modulated metasurface breaks reciprocity. To conserve the initial transverse momentum k_x in the time-reversed case, the presence of the frequency shift modifies the total momentum, and the reflected beam direction is thus given by $\sin\theta_{R,t\to-t} = \frac{k_\parallel c}{n(\omega+2\Delta\omega)}$. The red, green, and blue semicircles in Figure 8c represent equally spaced frequency curves (isofrequencies) corresponding to frequency values of ω, $\omega + \Delta\omega$, and $\omega + 2\Delta\omega$, respectively, to highlight the change in the length of the total momentum upon temporal modulation.[201]

Space and time modulated metasurface: for the general case of spatiotemporal modulation, space and time variations of phase-discontinuities change both the frequency and the tangential momentum of the reflected wave in the time forward scenario $t \to +t$, as illustrated in Figure 8b and c, bottom panels, providing more degrees of freedom in wavefront engineering. One way to achieve spatiotemporal modulation would consist in driving a homogeneous array at a given modulation frequency, making sure that each adjacent pillar is driven with an incremental, but fixed, modulation phase so as to introduce a spatial phase variation at a given time. The time-reversed process shows clearly that the spatiotemporally modulated metasurface breaks reciprocity. The bottom panel in Figure 8b reveals that oblique transitions are needed in (k_x, ω) space to change both the carrier frequency and the wave trajectory in the time-reversed process, leading to $\sin\theta_{R,t\to-t} = \frac{\omega}{\omega+2\Delta\omega}\sin\theta_{I,t\to+t}$. Note that the angle in the time-reversed case is not affected by the space gradient, simply because time-reversal symmetry breaking responsible for nonreciprocity is due to the time modulation that changes the normal momentum component.[201] In the case of a fixed phase period and uniform temporal modulation, the spatial variations of the phase discontinuities are thus not affecting the time-reversed process, but they can be utilized to address the beam in an arbitrary direction in the $t \to +t$. In the examples provided in Figure 8b,c, a nonreciprocal response in the spatial domain requires an incoming wave impinging on the metasurface at oblique incidence. However, some cases discussing nonreciprocity upon normal incidence on a time-modulated metasurfaces have been reported.[218,219] Finally, the most general case which could consist in arbitrary temporal modulation of each nanoelement taken independently, that is, not a fixed relative phase between adjacent elements, may provide essentially unlimited wavefront engineering capabilities in both spatial and frequency domains.

We find it interesting to highlight the difference between metasurfaces that provide asymmetric trajectories as a comparison to metasurfaces presenting nonreciprocal responses. An asymmetric metasurface is a device that deflects light at two different output angles, depending on the direction of illumination. This is the case of any basic phase gradient metasurface disposed at an interface between two media, as it breaks parity-symmetry after inverting the spatial coordinate ($z \to -z$). However, achieving nonreciprocity requires asymmetry upon time reversal.[205] Metasurfaces featuring bianisotropy are, in general, associated with asymmetric responses. These bianisotropic metasurfaces are dictated by magnetoelectric coupling holding for the excitation of a magnetic (electric) dipole moment by an electric (magnetic) field, leading to anisotropic responses. A solid review highlighting the physics and some interesting aspects of the bianisotropic metasurfaces can be found in ref 220. A very characteristic class of bianisotropic metasurfaces encompasses the so-called "chiral" ones. While we often read about planar chiral structures, chirality can only be achieved in three-dimensional space.[221] Therefore, chiral metasurfaces were mainly proposed as cascaded systems. As an example, we report on a bianisotropic metasurface based on superimposed gold sheets that have demonstrated asymmetric transmission through full polarization control of circularly polarized light. In that case, a Faraday rotation-like behavior has been witnessed through a magnetic-free approach.[222] Chiral building blocks belong to the so-called reciprocal bianisotropic meta-atoms since no external bias is employed. Interestingly, the bianisotropic coupling has been proposed for engineering nonreciprocal effects relying on the action of external stimuli. Very representative classes of nonreciprocal bianisotropic metasurfaces are the "Tellegen" and the so-called "moving" metasurfaces, generally comprising transistor-loaded structures. Ra'di et al.[223] proposed a magnet-free Tellegen metasurface that scatters the light asymmetrically when the device is

https://doi.org/10.1021/acsphotonics.1c01833
ACS Photonics XXXX, XXX, XXX−XXX

illuminated from different sides. "Moving" bianisotropic metasurfaces have also been introduced for achieving nonreciprocity. When we are talking about these "moving" metasurfaces, we do not mean that our metasurface is in motion. In practice, such metasurfaces may be engineered to incorporate bianisotropy that mimics the behavior of a moving medium.[223,224] In their recent publication, Rad'i and Alu explained that stationary inclusions can be engineered to electromagnetically move toward or against the observer, depending on the direction of the observation.[225] They conceptualized a metagrating designed to perform electromagnetic circulation between three channels. Further perspectives in tunable metasurface-based nonreciprocal devices are expected through the combination of bianisotropy and time-only modulation, as has been recently proposed by Wang et al.[226] Such a combination may serve at increasing the number of degrees of freedom in designing active nonreciprocal devices by leveraging on bianisotropic properties.[220]

We conclude that the important progress and advances in the tuning mechanisms reported in this Perspective are promising for fueling the engines to take off the industrial development of metasurfaces. About one decade ago, passive metasurfaces promised and succeeded in revolutionizing our ability to engineer electromagnetic waves, current tunable metasurfaces are bound to play a leading role in the industrialization of disruptive photonic systems. Space and time modulations with metasurfaces still have to address several challenges and difficulties. Notably, dedicated research efforts are needed to bring the architectures at optical frequencies, to better integrate and design the electronic drivers, to achieve high efficiency and high modulation performances through optimal design and processes, to develop sophisticated software, and to package complex and high density electronic circuitry on a chip-scale system. Additionally, benchmarking, device testing in real operational conditions, and design optimization are also required to demonstrate the reliability of the modulators for applications in AR/VR, LiDARs, and communications. Beyond the huge industrial interest, there is still a lot of space for fundamental research to both tackle existing bottlenecks as well as to foster conceptualization of novel physical phenomena. In particular, the unexplored field of time-modulated nonreciprocal metasurfaces at optical frequencies is expected to grow significantly in the coming years, offering new application perspectives. Finally, besides the fascinating physical effects and their potential implementation in new optical architectures, simple versions of time-modulated metasurfaces will be utilized to adapt and adjust the optical response of interfaces to operate at various on-demand wavelengths. The road that leads to the realization of an ultimate ultrafast and ultrathin nonreciprocal optical component is certainly challenging, but the perspectives of innovation along the road are extremely exciting. Various approaches considered in this manuscript have the potential to impact the field of photonics in both academic and industrial sectors, offering researchers working in this area an unlimited source of inspiration and innovations.

AUTHOR INFORMATION

Corresponding Author

Patrice Genevet − *Université Côte d'Azur, CNRS, CRHEA, 06560 Valbonne, France;* orcid.org/0000-0003-0216-3885; Email: pg@crhea.cnrs.fr

Authors

Elena Mikheeva − *Université Côte d'Azur, CNRS, CRHEA, 06560 Valbonne, France;* orcid.org/0000-0002-1831-2809

Christina Kyrou − *Université Côte d'Azur, CNRS, CRHEA, 06560 Valbonne, France*

Fouad Bentata − *Université Côte d'Azur, CNRS, CRHEA, 06560 Valbonne, France; Université de Lyon, Institut des Nanotechnologies de Lyon−INL, Ecully 69134, France; STMicroelectronics, 38920 Crolles, France*

Samira Khadir − *Université Côte d'Azur, CNRS, CRHEA, 06560 Valbonne, France*

Sébastien Cueff − *Université de Lyon, Institut des Nanotechnologies de Lyon−INL, Ecully 69134, France;* orcid.org/0000-0002-8668-2633

Complete contact information is available at: https://pubs.acs.org/10.1021/acsphotonics.1c01833

Author Contributions

‡These authors contributed equally to this work.

Funding

Bodossaki Foundation (Athens, Greece); French National Research Agency (ANR) project MetaOnDemand (ANR-20-CE24-0013); French National Research Agency (ANR) project Dilemma (ANR-20-CE09-0027).

Notes

The authors declare no competing financial interest.

ACKNOWLEDGMENTS

C.K. has been supported with a postdoctoral fellowship grant by the Bodossaki Foundation (Athens, Greece). E.M., F.B., S.C., and P.G. acknowledge support by the French National Research Agency (ANR) under the projects MetaOnDemand (ANR-20-CE24-0013) and Dilemma (ANR-20-CE09-0027).

REFERENCES

(1) Genevet, P.; Capasso, F.; Aieta, F.; Khorasaninejad, M.; Devlin, R. Recent advances in planar optics: from plasmonic to dielectric metasurfaces. *Optica* **2017**, *4*, 139−152.

(2) Chen, H.-T.; Taylor, A. J.; Yu, N. A review of metasurfaces: physics and applications. *Rep. Prog. Phys.* **2016**, *79*, 076401.

(3) Scheuer, J. Optical Metasurfaces Are Coming of Age: Short- and Long-Term Opportunities for Commercial Applications. *ACS Photonics* **2020**, *7*, 1323−1354.

(4) Sun, S.; He, Q.; Xiao, S.; Xu, Q.; Li, X.; Zhou, L. Gradient-index meta-surfaces as a bridge linking propagating waves and surface waves. *Nat. Mater.* **2012**, *11*, 426−431.

(5) Grady, N. K.; Heyes, J. E.; Chowdhury, D. R.; Zeng, Y.; Reiten, M. T.; Azad, A. K.; Taylor, A. J.; Dalvit, D. A. R.; Chen, H.-T. Terahertz Metamaterials for Linear Polarization Conversion and Anomalous Refraction. *Science* **2013**, *340*, 1304−1307.

(6) Song, Q.; Khadir, S.; Vézian, S.; Damilano, B.; Mierry, P. D.; Chenot, S.; Brandli, V.; Genevet, P. Bandwidth-unlimited polarization-maintaining metasurfaces. *Sci. Adv.* **2021**, *7*, No. eabe1112.

(7) Sawant, R.; Andrén, D.; Martins, R. J.; Khadir, S.; Verre, R.; Käll, M.; Genevet, P. Aberration-corrected large-scale hybrid metalenses. *Optica* **2021**, *8*, 1405−1411.

(8) Song, Q.; Baroni, A.; Wu, P. C.; Chenot, S.; Brandli, V.; Vézian, S.; Damilano, B.; de Mierry, P.; Khadir, S.; Ferrand, P.; Genevet, P. Broadband decoupling of intensity and polarization with vectorial Fourier metasurfaces. *Nat. Commun.* **2021**, *12*, 3631.

(9) Ren, H.; Briere, G.; Fang, X.; Ni, P.; Sawant, R.; Héron, S.; Chenot, S.; Vézian, S.; Damilano, B.; Brändli, V.; Maier, S. A.;

Genevet, P. Metasurface orbital angular momentum holography. *Nat. Commun.* **2019**, *10*, 2986.
(10) Zhang, L.; Chen, X. Q.; Liu, S.; Zhang, Q.; Zhao, J.; Dai, J. Y.; Bai, G. D.; Wan, X.; Cheng, Q.; Castaldi, G.; Galdi, V.; Cui, T. J. Space-time-coding digital metasurfaces. *Nat. Commun.* **2018**, *9*, 4334.
(11) Miroshnichenko, A. E.; Kivshar, Y. S. Polarization Traffic Control for Surface Plasmons. *Science* **2013**, *340*, 283−284.
(12) Arbabi, A.; Horie, Y.; Bagheri, M.; Faraon, A. Dielectric metasurfaces for complete control of phase and polarization with subwavelength spatial resolution and high transmission. *Nat. Nanotechnol.* **2015**, *10*, 937−943.
(13) Dorrah, A. H.; Rubin, N. A.; Zaidi, A.; Tamagnone, M.; Capasso, F. Metasurface optics for on-demand polarization transformations along the optical path. *Nat. Photonics* **2021**, *15*, 287−296.
(14) Leitis, A.; Tseng, M. L.; John-Herpin, A.; Kivshar, Y. S.; Altug, H. Wafer-Scale Functional Metasurfaces for Mid-Infrared Photonics and Biosensing. *Adv. Mater.* **2021**, *33*, 2102232.
(15) Luo, X.; Hu, Y.; Li, X.; Jiang, Y.; Wang, Y.; Dai, P.; Liu, Q.; Shu, Z.; Duan, H. Integrated Metasurfaces with Microprints and Helicity-Multiplexed Holograms for Real-Time Optical Encryption. *Adv. Opt. Mater.* **2020**, *8*, 1902020.
(16) Kwon, H.; Arbabi, E.; Kamali, S. M.; Faraji-Dana, M.; Faraon, A. Single-shot quantitative phase gradient microscopy using a system of multifunctional metasurfaces. *Nat. Photonics* **2020**, *14*, 109−114.
(17) Yu, N.; Genevet, P.; Kats, M. A.; Aieta, F.; Tetienne, J.-P.; Capasso, F.; Gaburro, Z. Light Propagation with Phase Discontinuities: Generalized Laws of Reflection and Refraction. *Science* **2011**, *334*, 333−337.
(18) Lalanne, P.; Astilean, S.; Chavel, P.; Cambril, E.; Launois, H. Blazed binary subwavelength gratings with efficiencies larger than those of conventional échelette gratings. *Opt. Lett.* **1998**, *23*, 1081−1083.
(19) Berry, M. The Adiabatic Phase and Pancharatnam's Phase for Polarized Light. *J. Mod. Opt.* **1987**, *34*, 1401−1407.
(20) Biener, G.; Niv, A.; Kleiner, V.; Hasman, E. Formation of helical beams by use of Pancharatnam−Berry phase optical elements. *Opt. Lett.* **2002**, *27*, 1875−1877.
(21) Song, Q.; Odeh, M.; Zúñiga-Pérez, J.; Kanté, B.; Genevet, P. Plasmonic topological metasurface by encircling an exceptional point. *Science* **2021**, *373*, 1133−1137.
(22) Kwon, H.; Sounas, D.; Cordaro, A.; Polman, A.; Alù, A. Nonlocal metasurfaces for optical signal processing. *Phys. Rev. Lett.* **2018**, *121*, 173004.
(23) Malek, S. C.; Overvig, A. C.; Alù, A.; Yu, N. Multifunctional Resonant Wavefront-Shaping Meta-Optics Based on Multilayer and Multi-Perturbation Nonlocal Metasurfaces. *arXiv:2009.07054 [physics.optics]* **2022**, na.
(24) Malek, S. C.; Overvig, A. C.; Shrestha, S.; Yu, N. Active nonlocal metasurfaces. *Nanophotonics* **2020**, *10*, 655−665.
(25) Song, J.-H.; van de Groep, J.; Kim, S. J.; Brongersma, M. L. Non-local metasurfaces for spectrally decoupled wavefront manipulation and eye tracking. *Nature Nanotechnol* **2021**, *16*, 1224−1230.
(26) Xie, Y.-Y.; Ni, P.-N.; Wang, Q.-H.; Kan, Q.; Briere, G.; Chen, P.-P.; Zhao, Z.-Z.; Delga, A.; Ren, H.-R.; Chen, H.-D.; Xu, C.; Genevet, P. Metasurface-integrated vertical cavity surface-emitting lasers for programmable directional lasing emissions. *Nat. Nanotechnol.* **2020**, *15*, 125−130.
(27) Wang, Q.-H.; Ni, P.-N.; Xie, Y.-Y.; Kan, Q.; Chen, P.-P.; Fu, P.; Deng, J.; Jin, T.-L.; Chen, H.-D.; Lee, H. W. H.; Xu, C.; Genevet, P. On-Chip Generation of Structured Light Based on Metasurface Optoelectronic Integration. *Laser Photonics Rev.* **2021**, *15*, 2000385.
(28) Arbabi, E.; Kamali, S. M.; Arbabi, A.; Faraon, A. Full-Stokes Imaging Polarimetry Using Dielectric Metasurfaces. *ACS Photonics* **2018**, *5*, 3132−3140.
(29) Mueller, J. P. B.; Leosson, K.; Capasso, F. Ultracompact metasurface in-line polarimeter. *Optica* **2016**, *3*, 42−47.
(30) Sievenpiper, D.; Schaffner, J.; Song, H.; Loo, R.; Tangonan, G. Two-dimensional beam steering using an electrically tunable impedance surface. *IEEE Trans. Antennas Propag.* **2003**, *51*, 2713−2722.
(31) Cui, T. J.; Qi, M. Q.; Wan, X.; Zhao, J.; Cheng, Q. Coding metamaterials, digital metamaterials and programmable metamaterials. *Light: Sci. Appl.* **2014**, *3*, No. e218.
(32) Watts, C. M.; Shrekenhamer, D.; Montoya, J.; Lipworth, G.; Hunt, J.; Sleasman, T.; Krishna, S.; Smith, D. R.; Padilla, W. J. Terahertz compressive imaging with metamaterial spatial light modulators. *Nat. Photonics* **2014**, *8*, 605−609.
(33) Zhu, W.; et al. A Flat Lens with Tunable Phase Gradient by Using Random Access Reconfigurable Metamaterial. *Adv. Mater.* **2015**, *27*, 4739−4743.
(34) Xu, H.-X.; Sun, S.; Tang, S.; Ma, S.; He, Q.; Wang, G.-M.; Cai, T.; Li, H.-P.; Zhou, L. Dynamical control on helicity of electromagnetic waves by tunable metasurfaces. *Sci. Rep.* **2016**, *6*, 27503.
(35) Li, L.; Jun Cui, T.; Ji, W.; Liu, S.; Ding, J.; Wan, X.; Bo Li, Y.; Jiang, M.; Qiu, C.-W.; Zhang, S. Electromagnetic reprogrammable coding-metasurface holograms. *Nat. Commun.* **2017**, *8*, 197.
(36) Chen, K.; Feng, Y.; Monticone, F.; Zhao, J.; Zhu, B.; Jiang, T.; Zhang, L.; Kim, Y.; Ding, X.; Zhang, S.; Alù, A.; Qiu, C.-W. A Reconfigurable Active Huygens' Metalens. *Adv. Mater.* **2017**, *29*, 1606422.
(37) Shao, L.; Zhu, W. Electrically Reconfigurable Microwave Metasurfaces With Active Lumped Elements: A Mini Review. *Frontiers in Materials* **2021**, *8*, 689665.
(38) Bang, S.; Kim, J.; Yoon, G.; Tanaka, T.; Rho, J. Recent Advances in Tunable and Reconfigurable Metamaterials. *Micromachines* **2018**, *9*, 560.
(39) He, Q.; Sun, S.; Zhou, L. Tunable/Reconfigurable Metasurfaces: Physics and Applications. *Research* **2019**, *2019*, 1.
(40) Nemati, A.; Wang, Q.; Hong, M.; Teng, J. Tunable and reconfigurable metasurfaces and metadevices. *Opto-Electron. Adv.* **2018**, *1*, 18000901.
(41) Lee, C.-W.; Choi, H. J.; Jeong, H. Tunable metasurfaces for visible and SWIR applications. *Nano Convergence* **2020**, *7*, 3.
(42) Shalaginov, M. Y.; Campbell, S. D.; An, S.; Zhang, Y.; Ríos, C.; Whiting, E. B.; Wu, Y.; Kang, L.; Zheng, B.; Fowler, C.; Zhang, H.; Werner, D. H.; Hu, J.; Gu, T. Design for quality: reconfigurable flat optics based on active metasurfaces. *Nanophotonics* **2020**, *9*, 3505−3534.
(43) Shaltout, A. M.; Shalaev, V. M.; Brongersma, M. L. Spatiotemporal light control with active metasurfaces. *Science* **2019**, *364*, No. eaat3100.
(44) Kang, L.; Jenkins, R. P.; Werner, D. H. Recent Progress in Active Optical Metasurfaces. *Adv. Opt. Mater.* **2019**, *7*, 1801813.
(45) Kim, I.; Martins, R. J.; Jang, J.; Badloe, T.; Khadir, S.; Jung, H.-Y.; Kim, H.; Kim, J.; Genevet, P.; Rho, J. Nanophotonics for light detection and ranging technology. *Nat. Nanotechnol.* **2021**, *16*, 508−524.
(46) Zhou, T.; Lin, X.; Wu, J.; Chen, Y.; Xie, H.; Li, Y.; Fan, J.; Wu, H.; Fang, L.; Dai, Q. Large-scale neuromorphic optoelectronic computing with a reconfigurable diffractive processing unit. *Nat. Photonics* **2021**, *15*, 367−373.
(47) Wuttig, M.; Bhaskaran, H.; Taubner, T. Phase-change materials for non-volatile photonic applications. *Nat. Photonics* **2017**, *11*, 465−476.
(48) Abdollahramezani, S.; Hemmatyar, O.; Taghinejad, H.; Krasnok, A.; Kiarashinejad, Y.; Zandehshahvar, M.; Alù, A.; Adibi, A. Tunable nanophotonics enabled by chalcogenide phase-change materials. *Nanophotonics* **2020**, *9*, 1189−1241.
(49) Ke, Y.; Wang, S.; Liu, G.; Li, M.; White, T. J.; Long, Y. Vanadium dioxide: The multistimuli responsive material and its applications. *Small* **2018**, *14*, 1802025.
(50) Cueff, S.; John, J.; Zhang, Z.; Parra, J.; Sun, J.; Orobtchouk, R.; Ramanathan, S.; Sanchis, P. VO_2 nanophotonics. *APL Photonics* **2020**, *5*, 110901.
(51) Ding, F.; Yang, Y.; Bozhevolnyi, S. I. Dynamic Metasurfaces Using Phase-Change Chalcogenides. *Adv. Opt. Mater.* **2019**, *7*, 1801709.

https://doi.org/10.1021/acsphotonics.1c01833
ACS Photonics XXXX, XXX, XXX−XXX

(52) Meng, Y.; Cao, T.; Long, Y. Progress in metasurfaces based on Ge−Sb−Te phase-change materials. *J. Appl. Phys.* **2020**, *128*, 140904.
(53) Zhang, Y.; Ríos, C.; Shalaginov, M. Y.; Li, M.; Majumdar, A.; Gu, T.; Hu, J. Myths and truths about optical phase change materials: A perspective. *Appl. Phys. Lett.* **2021**, *118*, 210501.
(54) Cueff, S.; Taute, A.; Bourgade, A.; Lumeau, J.; Monfray, S.; Song, Q.; Genevet, P.; Devif, B.; Letartre, X.; Berguiga, L. Reconfigurable Flat Optics with Programmable Reflection Amplitude Using Lithography-Free Phase-Change Material Ultra-Thin Films. *Adv. Opt. Mater.* **2021**, *9*, 2001291.
(55) Wan, C.; Zhang, Z.; Woolf, D.; Hessel, C. M.; Rensberg, J.; Hensley, J. M.; Xiao, Y.; Shahsafi, A.; Salman, J.; Richter, S.; Sun, Y.; Qazilbash, M. M.; Schmidt-Grund, R.; Ronning, C.; Ramanathan, S.; Kats, M. A.; et al. On the optical properties of thin-film vanadium dioxide from the visible to the far infrared. *Ann. Phys.* **2019**, *531*, 1900188.
(56) Zhang, Y.; et al. Electrically reconfigurable non-volatile metasurface using low-loss optical phase-change material. *Nat. Nanotechnol.* **2021**, *16*, 661−666.
(57) Teo, T. Y.; Krbal, M.; Mistrik, J.; Prikryl, J.; Lu, L.; Simpson, R. E. Comparison and analysis of phase change materials-based reconfigurable silicon photonic directional couplers. *Opt. Mater. Express* **2022**, *12*, 606−621.
(58) Lawson, D.; Hewak, D. W.; Muskens, O. L.; Zeimpekis, I. Time-resolved reversible optical switching of the ultralow-loss phase change material Sb_2Se_3. *J. Opt.* **2022**, na.
(59) Zhang, H.; Yang, X.; lu, L.; Chen, J.; Rahman, B. M. A.; Zhou, L.; et al. Comparison of the phase change process in a GST-loaded silicon waveguide and MMI. *Opt. Express* **2021**, *29*, 3503−3514.
(60) Delaney, M.; Zeimpekis, I.; Lawson, D.; Hewak, D. W.; Muskens, O. L. A New Family of Ultralow Loss Reversible Phase-Change Materials for Photonic Integrated Circuits: Sb_2S_3 and Sb_2Se_3. *Adv. Funct. Mater.* **2020**, *30*, 2002447.
(61) Dong, W.; Liu, H.; Behera, J. K.; Lu, L.; Ng, R. J.; Sreekanth, K. V.; Zhou, X.; Yang, J. K.; Simpson, R. E. Wide bandgap phase change material tuned visible photonics. *Adv. Funct. Mater.* **2019**, *29*, 1806181.
(62) Zhang, Y.; Chou, J. B.; Li, J.; Li, H.; Du, Q.; Yadav, A.; Zhou, S.; Shalaginov, M. Y.; Fang, Z.; Zhong, H.; Roberts, C.; Robinson, P.; Bohlin, B.; Rios, C.; Lin, H.; Kang, M.; Gu, T.; Warner, J.; Liberman, V.; Richardson, K.; Hu, J.; et al. Broadband transparent optical phase change materials for high-performance nonvolatile photonics. *Nat. Commun.* **2019**, *10*, 1−9.
(63) Imada, M.; Fujimori, A.; Tokura, Y. Metal-insulator transitions. *Rev. Mod. Phys.* **1998**, *70*, 1039.
(64) Cavalleri, A.; Tóth, C.; Siders, C. W.; Squier, J.; Ráksi, F.; Forget, P.; Kieffer, J. Femtosecond structural dynamics in VO_2 during an ultrafast solid-solid phase transition. *Phys. Rev. Lett.* **2001**, *87*, 237401.
(65) Jeong, Y.; Bahk, Y.; Kim, D. Dynamic Terahertz Plasmonics Enabled by Phase-Change Materials. *Adv. Opt. Mater.* **2020**, *8*, 1900548.
(66) Shabanpour, J.; Beyraghi, S.; Cheldavi, A. Ultrafast reprogrammable multifunctional vanadium-dioxide-assisted metasurface for dynamic THz wavefront engineering. *Sci. Rep.* **2020**, *10*, 8950.
(67) Rini, M.; Cavalleri, A.; Schoenlein, R. W.; López, R.; Feldman, L. C.; Haglund, R. F.; Boatner, L. A.; Haynes, T. E. Photoinduced phase transition in VO_2 nanocrystals: ultrafast control of surface-plasmon resonance. *Opt. Lett.* **2005**, *30*, 558−560.
(68) Cueff, S.; Li, D.; Zhou, Y.; Wong, F. J.; Kurvits, J. A.; Ramanathan, S.; Zia, R. Dynamic control of light emission faster than the lifetime limit using VO_2 phase-change. *Nat. Commun.* **2015**, *6*, 1−6.
(69) John, J.; Gutierrez, Y.; Zhang, Z.; Karl, H.; Ramanathan, S.; Orobtchouk, R.; Moreno, F.; Cueff, S. Multipolar resonances with designer tunability using VO_2 phase-change materials. *Phys. Rev. Appl.* **2020**, *13*, 044053.
(70) Howes, A.; Zhu, Z.; Curie, D.; Avila, J. R.; Wheeler, V. D.; Haglund, R. F.; Valentine, J. G. Optical Limiting Based on Huygens' Metasurfaces. *Nano Lett.* **2020**, *20*, 4638−4644.
(71) Kepic, P.; Ligmajer, F.; Hrton, M.; Ren, H.; Menezes, L. d. S.; Maier, S. A.; Sikola, T. Optically Tunable Mie Resonance VO_2 Nanoantennas for Metasurfaces in the Visible. *ACS Photonics* **2021**, *8*, 1048−1057.
(72) Tripathi, A.; John, J.; Kruk, S.; Zhang, Z.; Nguyen, H. S.; Berguiga, L.; Romeo, P. R.; Orobtchouk, R.; Ramanathan, S.; Kivshar, Y.; Cueff, S.; et al. Tunable Mie-Resonant Dielectric Metasurfaces Based on VO_2 Phase-Transition Materials. *ACS Photonics* **2021**, *8*, 1206−1213.
(73) Zhu, Z.; Evans, P. G.; Haglund, R. F., Jr; Valentine, J. G. Dynamically reconfigurable metadevice employing nanostructured phase-change materials. *Nano Lett.* **2017**, *17*, 4881−4885.
(74) Kim, Y.; Wu, P. C.; Sokhoyan, R.; Mauser, K.; Glaudell, R.; Kafaie Shirmanesh, G.; Atwater, H. A. Phase modulation with electrically tunable vanadium dioxide phase-change metasurfaces. *Nano Lett.* **2019**, *19*, 3961−3968.
(75) Butakov, N. A.; Knight, M. W.; Lewi, T.; Iyer, P. P.; Higgs, D.; Chorsi, H. T.; Trastoy, J.; Del Valle Granda, J.; Valmianski, I.; Urban, C.; Kalcheim, Y.; Wang, P. Y.; Hon, P. W. C.; Schuller, I. K.; Schuller, J. A. Broadband Electrically Tunable Dielectric Resonators Using Metal−Insulator Transitions. *ACS Photonics* **2018**, *5*, 4056−4060.
(76) Liu, Z.; Banar, B.; Butun, S.; Kocer, H.; Wang, K.; Scheuer, J.; Wu, J.; Aydin, K. Dynamic infrared thin-film absorbers with tunable absorption level based on VO $_2$ phase transition. *Opt. Mater. Express* **2018**, *8*, 2151.
(77) Dong, K.; Hong, S.; Deng, Y.; Ma, H.; Li, J.; Wang, X.; Yeo, J.; Wang, L.; Lou, S.; Tom, K. B.; Liu, K.; You, Z.; Wei, Y.; Grigoropoulos, C. P.; Yao, J.; Wu, J.; et al. A Lithography-Free and Field-Programmable Photonic Metacanvas. *Adv. Mater.* **2018**, *30*, 1703878.
(78) Liu, L.; Kang, L.; Mayer, T. S.; Werner, D. H. Hybrid metamaterials for electrically triggered multifunctional control. *Nat. Commun.* **2016**, *7*, 1−8.
(79) Cai, H.; Chen, S.; Zou, C.; Huang, Q.; Liu, Y.; Hu, X.; Fu, Z.; Zhao, Y.; He, H.; Lu, Y. Multifunctional hybrid metasurfaces for dynamic tuning of terahertz waves. *Adv. Opt. Mater.* **2018**, *6*, 1800257.
(80) Wuttig, M.; Deringer, V. L.; Gonze, X.; Bichara, C.; Raty, J.-Y. Incipient metals: functional materials with a unique bonding mechanism. *Adv. Mater.* **2018**, *30*, 1803777.
(81) Kooi, B. J.; Wuttig, M. Chalcogenides by design: Functionality through metavalent bonding and confinement. *Adv. Mater.* **2020**, *32*, 1908302.
(82) Raeis-Hosseini, N.; Rho, J. Metasurfaces Based on Phase-Change Material as a Reconfigurable Platform for Multifunctional Devices. *Materials* **2017**, *10*, 1046.
(83) Yang, H.; Xie, Z.; He, H.; Zhang, Q.; Li, J.; Zhang, Y.; Yuan, X. Switchable imaging between edge-enhanced and bright-field based on a phase-change metasurface. *Opt. Lett.* **2021**, *46*, 3741−3744.
(84) Yin, X.; Steinle, T.; Huang, L.; Taubner, T.; Wuttig, M.; Zentgraf, T.; Giessen, H. Beam switching and bifocal zoom lensing using active plasmonic metasurfaces. *Light: Sci. Appl.* **2017**, *6*, No. e17016.
(85) Tittl, A.; Michel, A.-K. U.; Schäferling, M.; Yin, X.; Gholipour, B.; Cui, L.; Wuttig, M.; Taubner, T.; Neubrech, F.; Giessen, H. A Switchable Mid-Infrared Plasmonic Perfect Absorber with Multispectral Thermal Imaging Capability. *Adv. Mater.* **2015**, *27*, 4597−4603.
(86) Wang, Q.; Rogers, E. T. F.; Gholipour, B.; Wang, C.-M.; Yuan, G.; Teng, J.; Zheludev, N. I. Optically reconfigurable metasurfaces and photonic devices based on phase change materials. *Nat. Photonics* **2016**, *10*, 60−65.
(87) Li, P.; Yang, X.; Maß, T. W. W.; Hanss, J.; Lewin, M.; Michel, A.-K. U.; Wuttig, M.; Taubner, T. Reversible optical switching of highly confined phonon−polaritons with an ultrathin phase-change material. *Nat. Mater.* **2016**, *15*, 870−875.

https://doi.org/10.1021/acsphotonics.1c01833
ACS Photonics XXXX, XXX, XXX−XXX

(88) Raoux, S.; Xiong, F.; Wuttig, M.; Pop, E. Phase change materials and phase change memory. *MRS Bull.* **2014**, *39*, 703−710.
(89) Cappelletti, P.; Annunziata, R.; Arnaud, F.; Disegni, F.; Maurelli, A.; Zuliani, P. Phase change memory for automotive grade embedded NVM applications. *J. Phys. D: Appl. Phys.* **2020**, *53*, 193002.
(90) Wang, Y.; Landreman, P.; Schoen, D.; Okabe, K.; Marshall, A.; Celano, U.; Wong, H.-S. P.; Park, J.; Brongersma, M. L. Electrical tuning of phase-change antennas and metasurfaces. *Nat. Nanotechnol.* **2021**, *16*, 667−672.
(91) Zheng, J.; Fang, Z.; Wu, C.; Zhu, S.; Xu, P.; Doylend, J. K.; Deshmukh, S.; Pop, E.; Dunham, S.; Li, M.; Majumdar, A. Nonvolatile Electrically Reconfigurable Integrated Photonic Switch Enabled by a Silicon PIN Diode Heater. *Adv. Mater.* **2020**, *32*, 2001218.
(92) Lepeshov, S.; Krasnok, A. Tunable phase-change metasurfaces. *Nat. Nanotechnol.* **2021**, *16*, 615−616.
(93) Abdollahramezani, S.; et al. Electrically driven programmable phase-change meta-switch reaching 80% efficiency. *arXiv:2104.10381 [physics.optics]* **2021**, na.
(94) Alvarez-Alegria, M.; Siegel, J.; Garcia-Pardo, M.; Cabello, F.; Toudert, J.; Haro-Poniatowski, E.; Serna, R. Nanosecond Laser Switching of Phase-Change Random Metasurfaces with Tunable ON-State. *Adv. Opt. Mater.* **2022**, *10*, 2101405.
(95) Fang, Z.; Zheng, J.; Saxena, A.; Whitehead, J.; Chen, Y.; Majumdar, A. Non-Volatile Reconfigurable Integrated Photonics Enabled by Broadband Low-Loss Phase Change Material. *Adv. Opt. Mater.* **2021**, *9*, 2002049.
(96) Hemmatyar, O.; Abdollahramezani, S.; Zeimpekis, I.; Lepeshov, S.; Krasnok, A.; Khan, A. I.; Neilson, K. M.; Teichrib, C.; Brown, T.; Pop, E.; Hewak, D. W.; Wuttig, M.; Alu, A.; Muskens, O. L.; Adibi, A. Enhanced Meta-Displays Using Advanced Phase-Change Materials. *arXiv:2107.12159 [physics.optics]* **2021**, na.
(97) Michel, A.-K. U.; Heßler, A.; Meyer, S.; Pries, J.; Yu, Y.; Kalix, T.; Lewin, M.; Hanss, J.; De Rose, A.; Maß, T. W. W.; Wuttig, M.; Chigrin, D. N.; Taubner, T.; et al. Advanced Optical Programming of Individual Meta-Atoms Beyond the Effective Medium Approach. *Adv. Mater.* **2019**, *31*, 1901033.
(98) Arnaud, F.; et al. Truly innovative 28nm FDSOI technology for automotive micro-controller applications embedding 16MB phase change memory. *IEEE Int. Electron Devices Meeting* **2018**, 18−4.
(99) Yu, S.; Wu, X.; Wang, Y.; Guo, X.; Tong, L. 2D Materials for Optical Modulation: Challenges and Opportunities. *Adv. Mater.* **2017**, *29*, 1606128.
(100) Ren, F.; Li, M.; Gao, Q.; Cowell, W.; Luo, J.; Jen, A. K.-Y.; Wang, A. X. Surface-normal plasmonic modulator using sub-wavelength metal grating on electro-optic polymer thin film. *Opt. Commun.* **2015**, *352*, 116−120.
(101) Zhang, J.; Kosugi, Y.; Otomo, A.; Ho, Y.-L.; Delaunay, J.-J.; Nakano, Y.; Tanemura, T. Electrical tuning of metal-insulator-metal metasurface with electro-optic polymer. *Appl. Phys. Lett.* **2018**, *113*, 231102.
(102) Karvounis, A.; Vogler-Neuling, V. V.; Richter, F. U.; Dénervaud, E.; Timofeeva, M.; Grange, R. Electro-Optic Metasurfaces Based on Barium Titanate Nanoparticle Films. *Adv. Opt. Mater.* **2020**, *8*, 2000623.
(103) Weigand, H.; Vogler-Neuling, V. V.; Escalé, M. R.; Pohl, D.; Richter, F. U.; Karvounis, A.; Timpu, F.; Grange, R. Enhanced Electro-Optic Modulation in Resonant Metasurfaces of Lithium Niobate. *ACS Photonics* **2021**, *8*, 3004−3009.
(104) Gao, B.; Ren, M.; Wu, W.; Cai, W.; Xu, J. Electro-optic lithium niobate metasurfaces. *Sci. China: Phys., Mech. Astron.* **2021**, *64*, 240362.
(105) Benea-Chelmus, I.-C.; Mason, S.; Meretska, M. L.; Elder, D. L.; Kazakov, D.; Shams-Ansari, A.; Dalton, L. R.; Capasso, F. *Gigahertz free-space electro-optic modulators based on Mie resonances*. 07.08.2021; ArXiv physics, DOI: 10.48550/arXiv.2108.03539, (accessed 2022-03−03).
(106) Kuo, Y.-H.; Lee, Y. K.; Ge, Y.; Ren, S.; Roth, J. E.; Kamins, T. I.; Miller, D. A. B.; Harris, J. S. Strong quantum-confined Stark effect in germanium quantum-well structures on silicon. *Nature* **2005**, *437*, 1334−1336.
(107) Wu, P. C.; Pala, R. A.; Kafaie Shirmanesh, G.; Cheng, W.-H.; Sokhoyan, R.; Grajower, M.; Alam, M. Z.; Lee, D.; Atwater, H. A. Dynamic beam steering with all-dielectric electro-optic III−V multiple-quantum-well metasurfaces. *Nat. Commun.* **2019**, *10*, 3654.
(108) Lee, J.; Jung, S.; Chen, P.-Y.; Lu, F.; Demmerle, F.; Boehm, G.; Amann, M.-C.; Alù, A.; Belkin, M. A. Ultrafast Electrically Tunable Polaritonic Metasurfaces. *Adv. Opt. Mater.* **2014**, *2*, 1057−1063.
(109) Monat, C.; Su, Y. Hybrid photonics beyond silicon. *APL Photonics* **2020**, *5*, 020402.
(110) Zhu, D.; Shao, L.; Yu, M.; Cheng, R.; Desiatov, B.; Xin, C. J.; Hu, Y.; Holzgrafe, J.; Ghosh, S.; Shams-Ansari, A.; Puma, E.; Sinclair, N.; Reimer, C.; Zhang, M.; Lončar, M. Integrated photonics on thin-film lithium niobate. *Adv. Opt. Photonics* **2021**, *13*, 242.
(111) Elshaari, A. W.; Pernice, W.; Srinivasan, K.; Benson, O.; Zwiller, V. Hybrid integrated quantum photonic circuits. *Nat. Photonics* **2020**, *14*, 285−298.
(112) Olivieri, A.; Chen, C.; Hassan, S.; Lisicka-Skrzek, E.; Tait, R. N.; Berini, P. Plasmonic Nanostructured Metal−Oxide−Semiconductor Reflection Modulators. *Nano Lett.* **2015**, *15*, 2304−2311.
(113) Iyer, P. P.; Pendharkar, M.; Schuller, J. A. Electrically Reconfigurable Metasurfaces Using Heterojunction Resonators. *Adv. Opt. Mater.* **2016**, *4*, 1582−1588.
(114) Liu, X.; Kang, J.-H.; Yuan, H.; Park, J.; Cui, Y.; Hwang, H. Y.; Brongersma, M. L. Tuning of Plasmons in Transparent Conductive Oxides by Carrier Accumulation. *ACS Photonics* **2018**, *5*, 1493−1498.
(115) Anopchenko, A.; Tao, L.; Arndt, C.; Lee, H. W. H. Field-Effect Tunable and Broadband Epsilon-Near-Zero Perfect Absorbers with Deep Subwavelength Thickness. *ACS Photonics* **2018**, *5*, 2631−2637.
(116) Howes, A.; Wang, W.; Kravchenko, I.; Valentine, J. Dynamic transmission control based on all-dielectric Huygens metasurfaces. *Optica* **2018**, *5*, 787.
(117) Alam, M. Z.; Schulz, S. A.; Upham, J.; De Leon, I.; Boyd, R. W. Large optical nonlinearity of nanoantennas coupled to an epsilon-near-zero material. *Nat. Photonics* **2018**, *12*, 79−83.
(118) Kafaie Shirmanesh, G.; Sokhoyan, R.; Pala, R. A.; Atwater, H. A. Dual-Gated Active Metasurface at 1550 nm with Wide (>300°) Phase Tunability. *Nano Lett.* **2018**, *18*, 2957−2963.
(119) Forouzmand, A.; Salary, M. M.; Inampudi, S.; Mosallaei, H. A Tunable Multigate Indium-Tin-Oxide-Assisted All-Dielectric Metasurface. *Adv. Opt. Mater.* **2018**, *6*, 1701275.
(120) Forouzmand, A.; Mosallaei, H. Electro-optical Amplitude and Phase Modulators Based on Tunable Guided-Mode Resonance Effect. *ACS Photonics* **2019**, *6*, 2860−2869.
(121) Lee, Y.; Yun, J.; Kim, S.; Seo, M.; In, S.; Jeong, H.; Lee, S.; Park, N.; Chung, T. D.; Lee, B. High-Speed Transmission Control in Gate-Tunable Metasurfaces Using Hybrid Plasmonic Waveguide Mode. *Adv. Opt. Mater.* **2020**, *8*, 2001256.
(122) Shirmanesh, G. K.; Sokhoyan, R.; Wu, P. C.; Atwater, H. A. Electro-optically Tunable Multifunctional Metasurfaces. *ACS Nano* **2020**, *14*, 6912−6920.
(123) Morea, M.; Zang, K.; Kamins, T. I.; Brongersma, M. L.; Harris, J. S. Electrically Tunable, CMOS-Compatible Metamaterial Based on Semiconductor Nanopillars. *ACS Photonics* **2018**, *5*, 4702−4709.
(124) Yan, H.; Low, T.; Zhu, W.; Wu, Y.; Freitag, M.; Li, X.; Guinea, F.; Avouris, P.; Xia, F. Damping pathways of mid-infrared plasmons in graphene nanostructures. *Nat. Photonics* **2013**, *7*, 394−399.
(125) Brar, V. W.; Jang, M. S.; Sherrott, M.; Lopez, J. J.; Atwater, H. A. Highly Confined Tunable Mid-Infrared Plasmonics in Graphene Nanoresonators. *Nano Lett.* **2013**, *13*, 2541−2547.
(126) Yao, Y.; Kats, M. A.; Genevet, P.; Yu, N.; Song, Y.; Kong, J.; Capasso, F. Broad Electrical Tuning of Graphene-Loaded Plasmonic Antennas. *Nano Lett.* **2013**, *13*, 1257−1264.

https://doi.org/10.1021/acsphotonics.1c01833
ACS Photonics XXXX, XXX, XXX−XXX

(127) Kim, T.-T.; Oh, S. S.; Kim, H.-D.; Park, H. S.; Hess, O.; Min, B.; Zhang, S. Electrical access to critical coupling of circularly polarized waves in graphene chiral metamaterials. *Sci. Adv.* **2017**, *3*, No. e1701377.
(128) Huang, Z.; Yao, K.; Su, G.; Ma, W.; Li, L.; Liu, Y.; Zhan, P.; Wang, Z. Graphene−metal hybrid metamaterials for strong and tunable circular dichroism generation. *Opt. Lett.* **2018**, *43*, 2636.
(129) Biswas, S. R.; Gutiérrez, C. E.; Nemilentsau, A.; Lee, I.-H.; Oh, S.-H.; Avouris, P.; Low, T. Tunable Graphene Metasurface Reflectarray for Cloaking, Illusion, and Focusing. *Phys. Rev. Appl.* **2018**, *9*, 034021.
(130) Han, S.; Kim, S.; Kim, S.; Low, T.; Brar, V. W.; Jang, M. S. Complete Complex Amplitude Modulation with Electronically Tunable Graphene Plasmonic Metamolecules. *ACS Nano* **2020**, *14*, 1166−1175.
(131) Sherrott, M. C.; Hon, P. W. C.; Fountaine, K. T.; Garcia, J. C.; Ponti, S. M.; Brar, V. W.; Sweatlock, L. A.; Atwater, H. A. Experimental Demonstration of > 230° Phase Modulation in Gate-Tunable Graphene−Gold Reconfigurable Mid-Infrared Metasurfaces. *Nano Lett.* **2017**, *17*, 3027−3034.
(132) Kim, S.; Jang, M. S.; Brar, V. W.; Mauser, K. W.; Kim, L.; Atwater, H. A. Electronically Tunable Perfect Absorption in Graphene. *Nano Lett.* **2018**, *18*, 971−979.
(133) Lee, H. W.; Papadakis, G.; Burgos, S. P.; Chander, K.; Kriesch, A.; Pala, R.; Peschel, U.; Atwater, H. A. Nanoscale Conducting Oxide PlasMOStor. *Nano Lett.* **2014**, *14*, 6463−6468.
(134) Park, J.; et al. All-solid-state spatial light modulator with independent phase and amplitude control for three-dimensional LiDAR applications. *Nat. Nanotechnol.* **2021**, *16*, 69−76.
(135) Davis, J.; Hsieh, Y.-H.; Lee, H.-C. Humans perceive flicker artifacts at 500 Hz. *Sci. Rep.* **2015**, *5*, 7861.
(136) Yu, P.; Li, J.; Zhang, S.; Jin, Z.; Schütz, G.; Qiu, C.-W.; Hirscher, M.; Liu, N. Dynamic Janus Metasurfaces in the Visible Spectral Region. *Nano Lett.* **2018**, *18*, 4584−4589.
(137) Li, J.; Kamin, S.; Zheng, G.; Neubrech, F.; Zhang, S.; Liu, N. Addressable metasurfaces for dynamic holography and optical information encryption. *Sci. Adv.* **2018**, *4*, No. eaar6768.
(138) Yu, P.; Li, J.; Li, X.; Schütz, G.; Hirscher, M.; Zhang, S.; Liu, N. Generation of Switchable Singular Beams with Dynamic Metasurfaces. *ACS Nano* **2019**, *13*, 7100−7106.
(139) Xu, T.; Walter, E. C.; Agrawal, A.; Bohn, C.; Velmurugan, J.; Zhu, W.; Lezec, H. J.; Talin, A. A. High-contrast and fast electrochromic switching enabled by plasmonics. *Nat. Commun.* **2016**, *7*, 10479.
(140) Peng, J.; Jeong, H.-H.; Lin, Q.; Cormier, S.; Liang, H.-L.; De Volder, M. F.; Vignolini, S.; Baumberg, J. J. Scalable electrochromic nanopixels using plasmonics. *Sci. Adv.* **2019**, *5*, No. eaaw2205.
(141) Kaissner, R.; Li, J.; Lu, W.; Li, X.; Neubrech, F.; Wang, J.; Liu, N. Electrochemically controlled metasurfaces with high-contrast switching at visible frequencies. *Sci. Adv.* **2021**, *7*, No. eabd9450.
(142) Chen, S.; Kang, E. S. H.; Shiran Chaharsoughi, M.; Stanishev, V.; Kühne, P.; Sun, H.; Wang, C.; Fahlman, M.; Fabiano, S.; Darakchieva, V.; Jonsson, M. P. Conductive polymer nanoantennas for dynamic organic plasmonics. *Nat. Nanotechnol.* **2020**, *15*, 35−40.
(143) Xiao, L.; Lv, Y.; Lin, J.; Hu, Y.; Dong, W.; Guo, X.; Fan, Y.; Zhang, N.; Zhao, J.; Wang, Y.; Liu, X. WO_3-Based Electrochromic Distributed Bragg Reflector: Toward Electrically Tunable Microcavity Luminescent Device. *Adv. Opt. Mater.* **2018**, *6*, 1700791.
(144) Ling, H.; Yeo, L. P.; Wang, Z.; Li, X.; Mandler, D.; Magdassi, S.; Tok, A. I. Y. TiO_2−WO_3 core−shell inverse opal structure with enhanced electrochromic performance in NIR region. *J. Mater. Chem. C* **2018**, *6*, 8488−8494.
(145) Li, Y.; van de Groep, J.; Talin, A. A.; Brongersma, M. L. Dynamic Tuning of Gap Plasmon Resonances Using a Solid-State Electrochromic Device. *Nano Lett.* **2019**, *19*, 7988−7995.
(146) Rosseinsky, D. R.; Mortimer, R. J. Electrochromic Systems and the Prospects for Devices. *Adv. Mater.* **2001**, *13*, 783−793.
(147) Andrén, D.; Baranov, D. G.; Jones, S.; Volpe, G.; Verre, R.; Käll, M. Microscopic metavehicles powered and steered by embedded optical metasurfaces. *Nat. Nanotechnol.* **2021**, *16*, 970−974.
(148) Badloe, T.; Lee, J.; Seong, J.; Rho, J. Tunable Metasurfaces: The Path to Fully Active Nanophotonics. *Advanced Photonics Research* **2021**, *2*, 2000205.
(149) Guanxing, Z.; Liu, Z.; Deng, W.; Zhu, W. Reconfigurable metasurfaces with mechanical actuations: towards flexible and tunable photonic devices. *Journal of Optics* **2021**, *23*, 013001.
(150) Chen, Y.; Ai, B.; Wong, Z. J. Soft optical metamaterials. *Nano Convergence* **2020**, *7*, 1−17.
(151) Chang, Y.; Wei, J.; Lee, C. Metamaterials − from fundamentals and MEMS tuning mechanisms to applications. *Nanophotonics* **2020**, *9*, 3049−3070.
(152) Algamili, A. S.; Khir, M. H. M.; Dennis, J. O.; Ahmed, A. Y.; Alabsi, S. S.; Hashwan, S. S. B.; Junaid, M. M. A review of actuation and sensing mechanisms in MEMS-based sensor devices. *Nanoscale Res. Lett.* **2021**, *16*, 1−21.
(153) Meng, C.; Thrane, P. C.; Ding, F.; Gjessing, J.; Thomaschewski, M.; Wu, C.; Dirdal, C.; Bozhevolnyi, S. I. Dynamic piezoelectric MEMS-based optical metasurfaces. *Sci. Adv.* **2021**, *7*, No. eabg5639.
(154) Bakke, T.; Vogl, A.; Żero, O.; Tyholdt, F.; Johansen, I.-R.; Wang, D. A novel ultra-planar, long-stroke and low-voltage piezoelectric micromirror. *J. Micromech. Microeng.* **2010**, *20*, 064010.
(155) Ren, Z.; Chang, Y.; Ma, Y.; Shih, K.; Dong, B.; Lee, C. Leveraging of MEMS technologies for optical metamaterials applications. *Adv. Opt. Mater.* **2020**, *8*, 1900653.
(156) Arbabi, E.; Arbabi, A.; Kamali, S. M.; Horie, Y.; Faraji-Dana, M.; Faraon, A. MEMS-tunable dielectric metasurface lens. *Nat. Commun.* **2018**, *9*, 1−9.
(157) Walia, S.; Shah, C. M.; Gutruf, P.; Nili, H.; Chowdhury, D. R.; Withayachumnankul, W.; Bhaskaran, M.; Sriram, S. Flexible metasurfaces and metamaterials: A review of materials and fabrication processes at micro- and nano-scales. *Appl. Phys. Rev.* **2015**, *2*, 011303.
(158) Kamali, S. M.; Arbabi, A.; Arbabi, E.; Horie, Y.; Faraon, A. Decoupling optical function and geometrical form using conformal flexible dielectric metasurfaces. *Nat. Commun.* **2016**, *7*, 1−7.
(159) Xu, H.-X.; Hu, G.; Wang, Y.; Wang, C.; Wang, M.; Wang, S.; Huang, Y.; Genevet, P.; Huang, W.; Qiu, C.-W. Polarization-insensitive 3D conformal-skin metasurface cloak. *Light: Sci. Appl.* **2021**, *10*, 1−13.
(160) Ee, H.-S.; Agarwal, R. Tunable metasurface and flat optical zoom lens on a stretchable substrate. *Nano Lett.* **2016**, *16*, 2818−2823.
(161) Chen, S.; Liu, Z.; Du, H.; Tang, C.; Ji, C.-Y.; Quan, B.; Pan, R.; Yang, L.; Li, X.; Gu, C.; Zhang, X.; Yao, Y.; Li, J.; Fang, N. X.; Li, J. Electromechanically reconfigurable optical nano-kirigami. *Nat. Commun.* **2021**, *12*, 1299.
(162) Wang, Z.; Jing, L.; Yao, K.; Yang, Y.; Zheng, B.; Soukoulis, C. M.; Chen, H.; Liu, Y. Origami-based reconfigurable metamaterials for tunable chirality. *Adv. Mater.* **2017**, *29*, 1700412.
(163) Han, Y.; Chen, S.; Ji, C.; Liu, X.; Wang, Y.; Liu, J.; Li, J. Reprogrammable optical metasurfaces by electromechanical reconfiguration. *Opt. Express* **2021**, *29*, 30751.
(164) Kim, J.; Rana, A. S.; Kim, Y.; Kim, I.; Badloe, T.; Zubair, M.; Mehmood, M. Q.; Rho, J. Chiroptical Metasurfaces: Principles, Classification, and Applications. *Sensors* **2021**, *21*, 4381.
(165) Probst, P. T.; Mayer, M.; Gupta, V.; Steiner, A. M.; Zhou, Z.; Auernhammer, G. K.; König, T. A. F.; Fery, A. Mechano-tunable chiral metasurfaces via colloidal assembly. *Nat. Mater.* **2021**, *20*, 1024−1028.
(166) Dahl-Hansen, R. P.; Tyholdt, F.; Gjessing, J.; Vogl, A.; Wittendorp, P.; Vedum, J.; Tybell, T. On the Effect of Water-Induced Degradation of Thin-Film Piezoelectric Microelectromechanical Systems. *J. Microelectromech. Syst.* **2021**, *30*, 105−115.
(167) Manjappa, M.; Pitchappa, P.; Singh, N.; Wang, N.; Zheludev, N. I.; Lee, C.; Singh, R. Reconfigurable MEMS Fano metasurfaces

https://doi.org/10.1021/acsphotonics.1c01833
ACS Photonics XXXX, XXX, XXX−XXX

with multiple-input−output states for logic operations at terahertz frequencies. *Nat. Commun.* **2018**, *9*, 4056.
(168) de Gennes, P.; Prost, J. *The Physics of Liquid Crystals*; International Series of Monographs on Physics, 1993.
(169) Kawamoto, H. The history of liquid-crystal displays. *Proc. IEEE* **2002**, *90*, 460−500.
(170) Otón, J. M.; Otón, E.; Quintana, X.; Geday, M. A. Liquid-crystal phase-only devices. *J. Mol. Liq.* **2018**, *267*, 469−483.
(171) Evans, P.; Wurtz, G.; Hendren, W.; Atkinson, R.; Dickson, W.; Zayats, A.; Pollard, R. Electrically switchable nonreciprocal transmission of plasmonic nanorods with liquid crystal. *Appl. Phys. Lett.* **2007**, *91*, 043101.
(172) Gorkunov, M. V.; Osipov, M. A. Tunability of wire-grid metamaterial immersed into nematic liquid crystal. *J. Appl. Phys.* **2008**, *103*, 036101.
(173) Kim, Y.; Won, K.; An, J.; Hong, J.-Y.; Kim, Y.; Choi, C.-S.; Song, H.; Song, B.; Kim, H. S.; Bae, K.-D.; Burm, J.; Lee, H.-S. Large-area liquid crystal beam deflector with wide steering angle. *Appl. Opt.* **2020**, *59*, 7462−7468.
(174) Xie, Z.-W.; Yang, J.-H.; Vashistha, V.; Lee, W.; Chen, K.-P. Liquid-crystal tunable color filters based on aluminum metasurfaces. *Opt. Express* **2017**, *25*, 30764−30770.
(175) Sharma, M.; Ellenbogen, T. An All-Optically Controlled Liquid-Crystal Plasmonic Metasurface Platform. *Laser Photonics Rev.* **2020**, *14*, 2000253.
(176) Atorf, B.; Mühlenbernd, H.; Zentgraf, T.; Kitzerow, H. All-optical switching of a dye-doped liquid crystal plasmonic metasurface. *Opt. Express* **2020**, *28*, 8898−8908.
(177) Bosch, M.; Shcherbakov, M. R.; Won, K.; Lee, H.-S.; Kim, Y.; Shvets, G. Electrically Actuated Varifocal Lens Based on Liquid-Crystal-Embedded Dielectric Metasurfaces. *Nano Lett.* **2021**, *21*, 3849−3856.
(178) Li, S.-Q.; Xu, X.; Maruthiyodan Veetil, R.; Valuckas, V.; Paniagua-Domínguez, R.; Kuznetsov, A. I. Phase-only transmissive spatial light modulator based on tunable dielectric metasurface. *Science* **2019**, *364*, 1087−1090.
(179) Li, J.; Yu, P.; Zhang, S.; Liu, N. Electrically-controlled digital metasurface device for light projection displays. *Nat. Commun.* **2020**, *11*, 3574.
(180) Zhu, S.; Xu, Z.; Zhang, H.; Yang, K.; Wang, N.; Liu, H.; Wang, Y.; Xia, J.; Huang, L. Liquid crystal integrated metadevice for reconfigurable hologram displays and optical encryption. *Opt. Express* **2021**, *29*, 9553−9564.
(181) Kim, I.; Kim, W.-S.; Kim, K.; Ansari, M. A.; Mehmood, M. Q.; Badloe, T.; Kim, Y.; Gwak, J.; Lee, H.; Kim, Y.-K.; Rho, J. Holographic metasurface gas sensors for instantaneous visual alarms. *Sci. Adv.* **2021**, *7*, No. eabe9943.
(182) Liu, Y.; Song, J.; Zhao, W.; Ren, X.; Cheng, Q.; Luo, X.; Fang, N. X.; Hu, R. Dynamic thermal camouflage via a liquid-crystal-based radiative metasurface. *Nanophotonics* **2020**, *9*, 855−863.
(183) Wu, J.; Shen, Z.; Ge, S.; Chen, B.; Shen, Z.; Wang, T.; Zhang, C.; Hu, W.; Fan, K.; Padilla, W.; Lu, Y.; Jin, B.; Chen, J.; Wu, P. Liquid crystal programmable metasurface for terahertz beam steering. *Appl. Phys. Lett.* **2020**, *116*, 131104.
(184) Shabanpour, J.; Sedaghat, M.; Nayyeri, V.; Oraizi, H.; Ramahi, O. M. Real-time multi-functional near-infrared wave manipulation with a 3-bit liquid crystal based coding metasurface. *Opt. Express* **2021**, *29*, 14525−14535.
(185) Ting, T.-L. Technology of liquid crystal based antenna. *Opt. Express* **2019**, *27*, 17138−17153.
(186) Sun, M.; Xu, X.; Sun, X. W.; Liang, X.; Valuckas, V.; Zheng, Y.; Paniagua-Domínguez, R.; Kuznetsov, A. I. Efficient visible light modulation based on electrically tunable all dielectric metasurfaces embedded in thin-layer nematic liquid crystals. *Sci. Rep.* **2019**, *9*, 8673.
(187) Su, H.; Wang, H.; Zhao, H.; Xue, T.; Zhang, J. Liquid-Crystal-Based Electrically Tuned Electromagnetically Induced Transparency Metasurface Switch. *Sci. Rep.* **2017**, *7*, 17378.
(188) Lininger, A.; Zhu, A. Y.; Park, J.-S.; Palermo, G.; Chatterjee, S.; Boyd, J.; Capasso, F.; Strangi, G. Optical properties of metasurfaces infiltrated with liquid crystals. *Proc. Natl. Acad. Sci. U. S. A.* **2020**, *117*, 20390−20396.
(189) Dolan, J. A.; Cai, H.; Delalande, L.; Li, X.; Martinson, A. B. F.; de Pablo, J. J.; López, D.; Nealey, P. F. Broadband Liquid Crystal Tunable Metasurfaces in the Visible: Liquid Crystal Inhomogeneities Across the Metasurface Parameter Space. *ACS Photonics* **2021**, *8*, 567−575.
(190) Xu, J.; Yang, R.; Fan, Y.; Fu, Q.; Zhang, F. A Review of Tunable Electromagnetic Metamaterials With Anisotropic Liquid Crystals. *Front. Phys.* **2021**, *9*, 67.
(191) Buchnev, O.; Podoliak, N.; Kaczmarek, M.; Zheludev, N. I.; Fedotov, V. A. Electrically Controlled Nanostructured Metasurface Loaded with Liquid Crystal: Toward Multifunctional Photonic Switch. *Adv. Opt. Mater.* **2015**, *3*, 674−679.
(192) Gorkunov, M. V.; Kasyanova, I. V.; Artemov, V. V.; Barnik, M. I.; Geivandov, A. R.; Palto, S. P. Fast Surface-Plasmon-Mediated Electro-Optics of a Liquid Crystal on a Metal Grating. *Phys. Rev. Applied* **2017**, *8*, 054051.
(193) Franklin, D.; Chen, Y.; Vázquez-Guardado, A.; Modak, S.; Boroumand, J.; Xu, D.; Wu, S.-T.; Chanda, D. Polarization-independent actively tunable colour generation on imprinted plasmonic surfaces. *Nat. Commun.* **2015**, *6*, 7337.
(194) Kowerdziej, R.; Wróbel, J.; Kula, P. Ultrafast electrical switching of nanostructured metadevice with dual-frequency liquid crystal. *Sci. Rep.* **2019**, *9*, 20367.
(195) Akselrod, G. M.; Yang, Y.; Bowen, P. Tunable liquid crystal metasurfaces. U.S. Patent 20200303826 A1, September 24, 2020.
(196) Ma, Y.; Tam, A. M. W.; Gan, X. T.; Shi, L. Y.; Srivastava, A. K.; Chigrinov, V. G.; Kwok, H. S.; Zhao, J. L. Fast switching ferroelectric liquid crystal Pancharatnam-Berry lens. *Opt. Express* **2019**, *27*, 10079−10086.
(197) Tsilipakos, O.; et al. Toward Intelligent Metasurfaces: The Progress from Globally Tunable Metasurfaces to Software-Defined Metasurfaces with an Embedded Network of Controllers. *Adv. Opt. Mater.* **2020**, *8*, 2000783.
(198) Zhang, W.; Mazzarello, R.; Wuttig, M.; Ma, E. Designing crystallization in phase-change materials for universal memory and neuro-inspired computing. *Nat. Rev. Mater.* **2019**, *4*, 150−168.
(199) Wu, C.; Yu, H.; Lee, S.; Peng, R.; Takeuchi, I.; Li, M. Programmable phase-change metasurfaces on waveguides for multimode photonic convolutional neural network. *Nat. Commun.* **2021**, *12*, 96.
(200) Kwon, H.; Zheng, T.; Faraon, A. Nano-electromechanical Tuning of Dual-Mode Resonant Dielectric Metasurfaces for Dynamic Amplitude and Phase Modulation. *Nano Lett.* **2021**, *21*, 2817−2823.
(201) Shaltout, A.; Kildishev, A.; Shalaev, V. Time-varying metasurfaces and Lorentz non-reciprocity. *Opt. Mater. Express* **2015**, *5*, 2459−2467.
(202) Achouri, K.; Caloz, C. *Electromagnetic Metasurfaces: Theory and Applications*; Wiley IEEE Press, 2021.
(203) Caloz, C.; Alù, A.; Tretyakov, S.; Sounas, D.; Achouri, K.; Deck-Léger, Z.-L. What is Nonreciprocity? *Phys. Rev. Appl.* **2018**, *10*, 047001.
(204) Asadchy, V. S.; Mirmoosa, M. S.; Díaz-Rubio, A.; Fan, S.; Tretyakov, S. A. Tutorial on Electromagnetic Nonreciprocity and its Origins. *Proc. IEEE* **2020**, *108*, 1684−1727.
(205) Caloz, C.; Alu, A.; Tretyakov, S.; Sounas, D.; Achouri, K.; Deck-Léger, Z.-L. Electromagnetic nonreciprocity. *Phys. Rev. Appl.* **2018**, *10*, 047001.
(206) Caloz, C.; Deck-Léger, Z.-L. Spacetime metamaterials—part I: general concepts. *IEEE Trans. Antennas Propag.* **2020**, *68*, 1569−1582.
(207) Caloz, C.; Deck-Léger, Z.-L. Spacetime metamaterials—part II: theory and applications. *IEEE Trans. Antennas Propag.* **2020**, *68*, 1583−1598.
(208) Maznev, A.; Every, A.; Wright, O. Reciprocity in reflection and transmission: What is a 'phonon diode'? *Wave Motion* **2013**, *50*, 776−784.
(209) Krasnok, A.; Tymchenko, M.; Alù, A. Nonlinear metasurfaces: a paradigm shift in nonlinear optics. *Mater. Today* **2018**, *21*, 8−21.

https://doi.org/10.1021/acsphotonics.1c01833
ACS Photonics XXXX, XXX, XXX−XXX

(210) Hadad, Y.; Sounas, D. L.; Alu, A. Space-time gradient metasurfaces. *Phys. Rev. B* **2015**, *92*, 100304.
(211) Taravati, S.; Eleftheriades, G. V. Full-duplex nonreciprocal beam steering by time-modulated phase-gradient metasurfaces. *Phys. Rev. Appl.* **2020**, *14*, 014027.
(212) Guo, X.; Ding, Y.; Duan, Y.; Ni, X. Nonreciprocal metasurface with space−time phase modulation. *Light: Sci. Appl.* **2019**, *8*, 1−9.
(213) Zhang, L.; Chen, X. Q.; Liu, S.; Zhang, Q.; Zhao, J.; Dai, J. Y.; Bai, G. D.; Wan, X.; Cheng, Q.; Castaldi, G.; Galdi, V.; Cui, T. J. Space-time-coding digital metasurfaces. *Nat. Commun.* **2018**, *9*, 4334.
(214) Zhang, L.; Chen, X. Q.; Shao, R. W.; Dai, J. Y.; Cheng, Q.; Castaldi, G.; Galdi, V.; Cui, T. J. Breaking Reciprocity with Space-Time-Coding Digital Metasurfaces. *Adv. Mater.* **2019**, *31*, 1904069.
(215) Liu, M.; Powell, D. A.; Zarate, Y.; Shadrivov, I. V. Huygens' Metadevices for Parametric Waves. *Phys. Rev. X* **2018**, *8*, 031077.
(216) Liu, B.; Wong, S.-W.; Li, Y. Rotational Doppler effect by space-time-coding metasurfaces for nonreciprocal electromagnetic isolation. *Opt. Express* **2021**, *29*, 24500−24507.
(217) Taravati, S.; Eleftheriades, G. V. Four-dimensional wave transformations by space-time metasurfaces. *arXiv:2011.08423 [physics.app-ph]* **2020**, na.
(218) Shi, Y.; Fan, S. Dynamic non-reciprocal meta-surfaces with arbitrary phase reconfigurability based on photonic transition in meta-atoms. *Appl. Phys. Lett.* **2016**, *108*, 021110.
(219) Wang, X.; Caloz, C. Advances in Spacetime-Modulated Metasurfaces. *2020 XXXIIIrd General Assembly and Scientific Symposium of the International Union of Radio Science - URSI GASS 2020*, Rome, Italy, Aug. 29 - Sept. 5, 2020, URSI, 2020; pp 1−3.
(220) Asadchy, V. S.; Díaz-Rubio, A.; Tretyakov, S. A. Bianisotropic metasurfaces: physics and applications. *Nanophotonics* **2018**, *7*, 1069−1094.
(221) Caloz, C.; Sihvola, A. Electromagnetic Chirality, Part 1: The Microscopic Perspective [Electromagnetic Perspectives]. *IEEE Antennas and Propagation Magazine* **2020**, *62*, 58−71.
(222) Pfeiffer, C.; Zhang, C.; Ray, V.; Guo, L. J.; Grbic, A. High Performance Bianisotropic Metasurfaces: Asymmetric Transmission of Light. *Phys. Rev. Lett.* **2014**, *113*, 023902.
(223) Ra'di, Y.; Grbic, A. Magnet-free nonreciprocal bianisotropic metasurfaces. *Phys. Rev. B* **2016**, *94*, 195432.
(224) Ramaccia, D.; Sounas, D. L.; Alù, A.; Toscano, A.; Bilotti, F. Phase-induced frequency conversion and doppler effect with time-modulated metasurfaces. *IEEE Trans. Antennas Propag.* **2020**, *68*, 1607−1617.
(225) Ra'di, Y.; Alù, A. Nonreciprocal Wavefront Manipulation in Synthetically Moving Metagratings. *Photonics* **2020**, *7* (2), 28.
(226) Wang, X.; Ptitcyn, G.; Asadchy, V. S.; Díaz-Rubio, A.; Mirmoosa, M. S.; Fan, S.; Tretyakov, S. A. Nonreciprocity in Bianisotropic Systems with Uniform Time Modulation. *Phys. Rev. Lett.* **2020**, *125*, 266102.

https://doi.org/10.1021/acsphotonics.1c01833
ACS Photonics XXXX, XXX, XXX−XXX